# An enhanced stochastic operating cycle description including weather and traffic models

(article starts on next page)

# An enhanced stochastic operating cycle description including weather and traffic models

Luigi Romano [a,*], Pär Johannesson [b], Fredrik Bruzelius [a,c], Bengt Jacobson [a]

[a] *Department of Mechanics and Maritime Sciences, Chalmers University of Technology, Hörsalsvägen 7A, 412 96 Gothenburg, Sweden*
[b] *RISE Research Institutes of Sweden, Gibraltargatan 35, 412 79 Gothenburg, Sweden*
[c] *Driver and Vehicle, VTI Swedish National Road and Transport Research Institute, Box 8072, 402 78 Gothenburg, Sweden*

A B S T R A C T

The present paper extends the concept of a stochastic operating cycle (sOC) by introducing additional models for weather and traffic. In regard to the weather parameters, dynamic models for air temperature, atmospheric pressure, relative humidity, precipitation, wind speed and direction are included. The traffic models is instead based on a macroscopic approach which describes the density dynamically by means of a simple autoregressive process. The enhanced format is structured in a hierarchical fashion, allowing for ease of implementation and modularity. The novel models are parametrised starting from data available from external databases. The possibility of generating synthetic data using the statistical descriptors introduced in the paper is also discussed.

To investigate the impact of the novel parameters over energy efficiency, a sensitivity analysis is conducted with a combinatorial test design. Simulation results show that both seasonality and traffic conditions are responsible for introducing major variations in the $CO_2$ emissions.

## 1. Introduction

Several sources highlight the incontestable nature of an anthropogenic cause of climate change. To cite a few, one might look at the technical reports authored by Hausfather (2020), Callery (2019), and those drafted by the Union of concerned scientists (2019), European Environmental Agency (2019), C.C.C. Service(2019), U.S.E.P. Agency(2019), Eurostat (2019), G.C. Project (2017). A conspicuous contribution comes from the release of equivalent $CO_2$ emissions from human activity relating to the transportation sector. This incentivised the European Commission (2014b), European Commission (2014a), European Commission (2017) to adopt several strict measures contrasting the alarming trend of increasing temperature and pollution. More specifically, emission thresholds have been set for heavy-duty and passenger vehicles. Preliminary tests are aimed at ensuring compliance with these limits and can be carried out physically or by using simulation tools. Different models and platforms have been developed to serve this purpose.

For example, the VT-Micro tool Rakha et al. (2004) is a regression model which is able to estimate with great precision the pollutant emissions of light and heavy-duty vehicles depending on their usage. More specifically, VT-Micro makes uses of statistical clustering techniques to group vehicles into homogeneous categories. The microscopic models are thus developed by aggregating non-steady-state emissions data based on both the vehicles' characteristics and the operational conditions.

Vehicular efficiency may also be assessed by simulation in virtual environments. This is usually done at a very early stage avoiding

* Corresponding author.
  *E-mail address:* luigi.romano@chalmers.se (L. Romano).

**Nomenclature**

| | |
|---|---|
| $A$ | Effective frontal area $\mathrm{m^2}$ |
| $C_\mathrm{d}$ | Drag coefficient $\mathrm{N\,m^{-2}}$ |
| $F_x$ | Longitudinal force N |
| $F_\mathrm{air}$ | Air resistance N |
| $F_\mathrm{b}$ | Brake force N |
| $F_\mathrm{grade}$ | Grade resistance N |
| $F_\mathrm{inertia}$ | Inertial force N |
| $F_\mathrm{roll}$ | Rolling resistance N |
| $H_\mathrm{p}$ | Random variable for precipitation occurrence mm |
| $P_\mathrm{drive}$ | Power for driving W |
| $\mathbf{P}_H$ | Markov matrix for precipitation occurrence – |
| $P_\mathrm{PTO}$ | Power take-off W |
| $P_\mathrm{tot}$ | Total power W |
| $P_\mathrm{air}$ | Random variable for atmospheric pressure W |
| $R$ | Ideal gas constant $\mathrm{kJ\,kg^{-1}\,K^{-1}}$ |
| $R_\mathrm{w}$ | Wheel radius m |
| $T_\mathrm{air}$ | Air temperature $^\circ$C |
| $T_\mathrm{b}, T_\mathrm{d}$ | Brake and driving torques (Appendix A) $\mathrm{N\,m}$ |
| $T_\mathrm{b}^\mathrm{max}$ | Maximum brake torque $\mathrm{N\,m}$ |
| $T_\mathrm{d}, T_\mathrm{y}$ | Daily and annual amplitudes of temperature $^\circ$C |
| $T_\mathrm{e}$ | Engine torque $\mathrm{N\,m}$ |
| $\widetilde{T}$ | Random variable for air temperature $^\circ$C |
| $V_\mathrm{w}$ | Random variable for wind velocity (magnitude) $\mathrm{km\,h^{-1}}$ |
| $Y_\mathrm{w}$ | Random vector variable for wind speed and direction $\mathrm{km\,h^{-1}}$, rad |
| $c_P$ | Constant term for pressure autoregressive model hPa |
| $c_\mathrm{f}$ | Mass of $CO_2$ per mass of fuel $\mathrm{g_{CO_2}\,mg_f^{-1}}$ |
| $a_\mathrm{p}$ | Accelerator pedal position – |
| $a_x^\mathrm{max}$ | Maximum acceleration $\mathrm{m\,s^{-2}}$ |
| $b_\mathrm{p}$ | Brake pedal position – |
| $c_\mathrm{w}$ | Constant term for wind autoregressive model $\mathrm{km\,h^{-1}}$, rad |
| $d_\mathrm{d}$ | Daily ceiling operator – |
| $d_\mathrm{y}$ | Annual ceiling operator – |
| $e_T$ | Error term for air temperature $^\circ$C |
| $e_P$ | Error term for atmospheric pressure hPa |
| $e_\mathrm{w}$ | Error term for wind speed and direction $\mathrm{km\,h^{-1}}$, rad |
| $e_\rho$ | Error term for traffic density $\mathrm{km^{-1}}$ |
| $e_\psi$ | Error term for relative humidity % |
| $f_{Hij}$ | Number of observed transitions (precipitation occurrence) – |
| $f_\mathrm{r}$ | Rolling resistance coefficient – |
| $h_\mathrm{p}$ | Precipitation amount (realisation) mm |
| $i_\mathrm{g}$ | Gear ratio – |
| $i_\mathrm{FD}$ | Final drive gear – |
| $m$ | Total mass kg |
| $m^*$ | Total mass including reduced rotational inertias kg |
| $m_\mathrm{f}$ | Fuel mass mg |
| $p_\mathrm{air}$ | Atmospheric pressure hPa |
| $p_{Hij}$ | Markov matrix entries for precipitation occurrence – |
| $q$ | Fuel injection mg |
| $q_\mathrm{e}$ | Equilibrium flow h |
| $t$ | Time s |
| $v_x$ | Longitudinal speed $\mathrm{m\,s^{-1}}$ |
| $v_\mathrm{b}$ | Speed bump $\mathrm{km\,h^{-1}}$ |
| $v_\mathrm{d}$ | Driver's desired speed $\mathrm{km\,h^{-1}}$ |
| $v_\mathrm{e}$ | Equilibrium speed $\mathrm{km\,h^{-1}}$ |
| $v_\mathrm{f}$ | Free-flow speed $\mathrm{km\,h^{-1}}$ |

| $v_{\text{sign}}$ | Legal speed sign $\text{km}\,\text{h}^{-1}$ |
|---|---|
| $v_{\text{stop}}$ | Stop speed $\text{km}\,\text{h}^{-1}$ |
| $v_{\text{t}}$ | Traffic speed $\text{km}\,\text{h}^{-1}$ |
| $\boldsymbol{v}_{\text{w}}, v_{\text{w}}$ | Wind velocity vector and magnitude $\text{km}\,\text{h}^{-1}$ |
| $v_{\kappa}$ | Curvature speed $\text{km}\,\text{h}^{-1}$ |
| $x, x_i$ | Longitudinal position, regressors m, – |
| $y$ | Response variable – |
| $\Theta_{\text{w}}$ | Random variable for wind direction rad |
| $\boldsymbol{\Phi}_{\text{w}j}$ | Autoregressive matrices for wind speed and direction $\text{km}\,\text{h}^{-1}, \text{km}^{-1}\,\text{h}$ |
| $\widetilde{\Psi}$ | Random variable for relative humidity % |
| $\Lambda$ | Random variable for precipitation intensity mm |
| $\boldsymbol{\Sigma}_{e_{\text{w}}}$ | Covariance matrix for wind speed and direction $\text{km}^2\,\text{h}^{-2}, \text{km}\,\text{h}^{-1}, \text{rad}^2$ |
| $\alpha$ | Road slope angle rad |
| $\alpha_{\Lambda_{\text{p}}}$ | Random variable for relative humidity – |
| $\beta_i, \beta_{ij}$ | Linear regression coefficient – |
| $\beta_{\Lambda_{\text{p}}}$ | Random variable for relative humidity $\text{mm}^{-1}$ |
| $\gamma$ | Proportionality constant – |
| $\varepsilon$ | Residual % |
| $\eta_{\text{t}}$ | Transmission efficiency – |
| $\kappa$ | Road curvature $\text{m}^{-1}$ |
| $\mu_T$ | Mean temperature $^\circ\text{C}$ |
| $\mu_\Psi$ | Mean relative humidity – |
| $\mu_{\Theta_{\text{w}}}$ | Mean wind direction rad |
| $\mu_\rho$ | Mean traffic density $\text{km}^{-1}$ |
| $\rho_{\text{air}}$ | Air density $\text{kg}\,\text{m}^{-3}$ |
| $\rho_{\text{c}}$ | Critical traffic density $\text{km}^{-1}$ |
| $\rho_{\text{d}}$ | Daily traffic density amplitude $\text{km}^{-1}$ |
| $\rho_{\text{t}}$ | Traffic density $\text{km}^{-1}$ |
| $\phi_{Pj}$ | Autoregressive coefficients for atmospheric pressure – |
| $\phi_T$ | Autoregressive coefficient for air temperature – |
| $\phi_\Psi$ | Autoregressive coefficient for relative humidity – |
| $\phi_\rho$ | Autoregressive coefficient for traffic density – |
| $\varphi_{T_{\text{d}}}, \varphi_{T_{\text{y}}}$ | Initial phases for air temperature rad |
| $\varphi_{\Psi_{\text{d}}}, \varphi_{\Psi_{\text{y}}}$ | Initial phases for relative humidity rad |
| $\varphi_\rho$ | Initial phase for traffic density rad |
| $\sigma^2_{e_P}$ | Atmospheric pressure innovation variance – |
| $\sigma^2_{e_T}$ | Air temperature innovation variance $^\circ\text{C}^2$ |
| $\sigma^2_{e_\Psi}$ | Relative humidity innovation variance – |
| $\sigma^2_{e_\rho}$ | Traffic density innovation variance $\text{km}^{-2}$ |
| $\omega_e$ | Engine speed $\text{rad}\,\text{s}^{-1}$ |

the construction and testing of physical prototypes. In this context, the $CO_2$ emissions and energy consumption of road vehicles are often estimated and compared using reference speed and elevation profiles, known as *driving cycles*, in conjunction with simplified models of longitudinal dynamics Guzzella and Sciarretta (2013). In particular, there exist two main variants of a driving cycle: modal and transient. The former type is usually used in standard tests regulated by legislation, since it allows for straightforward and fair comparison. With reference to heavy-duty vehicles, for example, the European Commission (2019) has considered adopting a virtual testing environment, called VECTO, as a certification tool for new concepts to be brought to the market Fontaras et al. (2013).

Two other popular types of emissions model which make analogous use of driving cycles are the Comprensive Modal Emission Model (CMEM)[1] and the Vehicle Specific Power (VSP)-based model represented by MOVES [2]. CMEM uses a power-demand approach based on a parametric description of fuel consumption and emissions. Individual contributions to these are allocated to components corresponding to physical phenomena associated with specific operational conditions. In turn, each component is modelled analytically using a multitude of parameters which correlate with the process. These parameters vary according to the vehicle type, engine,

---

[1] Additional information available from: https://www.cert.ucr.edu/cmem.
[2] Additional information available from: https://nepis.epa.gov/Exe/ZyPDF.cgi?Dockey=P1001DAQ.pdf.

emission technology and level of deterioration. A similar strategy is used in the VSP-model, which calculates the power demand on the engine starting from the second-by-second speed values in a driving schedule, plus information about the type of vehicle being operated.

Nevertheless, a major criticism of modal driving cycles is that they are not very realistic and are rapidly becoming obsolete. Therefore, many efforts have been devoted to replace them with transient cycles, as seen in Perugu et al. (2019). Transient cycles are also preferred for powertrain optimisation and design purposes requiring accurate feasibility studies, such as those conducted by Ghandriz et al. (2016), Ghandriz (2018), Ghandriz et al. (2020), Asbogaard et al. (2007). In this context, a crucial aspect of efficient design is the accurate description of a transport operation, with exhaustive information about the surroundings. Indeed, to correctly replicate real-world performance, it is necessary to take into account all the external factors and stimuli which may affect the vehicle's behaviour. These include road and mission properties, but also weather and traffic conditions Wyatt et al. (2014), Sentoff et al. (2015), Llopis-Castello et al. (2018), Sciarretta (2020).

## 1.1. Previous works on driving and operating cycles

How to synthesise representative transient cycles is an interesting and open question, and different approaches have been proposed in the literature. In particular, it is possible to distinguish between rule-based methods and statistical ones. Rule-based methods are very sensitive to experts' opinion and aim to replicate a limited number of characteristics from the measured driving cycles Zou et al. (2004), Naghizadeh (2003). Such a criterion may be represented by the percentages of city, suburb and highway speeds.

By contrast, the advantage of resorting to statistical techniques resides in the fact that generated synthetic speed profiles correlate with certain operating conditions of the vehicle, such as cruising, idling, acceleration or braking events. This enhanced approach combines different information (mostly inferred by speed and acceleration signals) to reflect the characteristics of real driving scenarios Nyberg (2015), Ashatari et al. (2014), Tazelaar et al. (2009), Lin and Niemeier (2002), Brady and O'Mahony (2016), Lee and Filipi (2011), Lee et al. (2011), Amirjamshidi and Roorda (2015), Kamble et al. (2009), Silvas (2015), Silvas et al. (2016).

More specifically, four different methods have been proposed to construct synthetic driving cycles: micro-trip based, segment-based, pattern classification and modal cycle construction Liu et al. (2020). In the micro-trip based method, several candidate cycles are firstly generated from micro-trips. These are defined as excursions between two subsequent stops and may be chosen either randomly or based on specific modal characteristics. The optimal cycle is finally selected based on the fulfillment of some satisfaction criterion, using a genetic algorithm for example Shi et al. (2009), Liu et al. (2008). Driving cycles have been synthesised with the micro-trip based methods for the cities of Hong Kong Hung et al. (2007), Pune and Chennai, India, Kamble et al. (2009), Nesamani and Subramanian (2011) and Singapore Ho et al. (2014).

In the segment-based method, a driving cycle is constructed from measured signals which are partitioned considering not only consecutive stops, but also the road characteristics and traffic conditions Sciarretta (2020). Segments may therefore begin and end at any speed. A related difficulty resides in that constraints on speed and acceleration must be imposed in chaining the segments together when synthesising a new cycle Kivekas et al. (2018), Kivekas et al. (2017).

The pattern classification method partitions the speed data into kinematic sequences similar to microtrips (Guo and Zhang, 2016; Ou et al., 2011; Berzi et al., 2016). With the aid of statistical techniques, these are then classified into heterogeneous classes depending on some defined criteria. The final driving cycle is thus synthesised combining the kinematic sequences based on the statistical properties of the classes. In several studies, new cycles have been synthesised from kinematics sequences using principal component analysis (PCA) and cluster analysis Jing et al. (2017).

In the modal cycle method, the measured speed data is clustered into snippets and classified into modal bins by using maximum likelihood estimation Lin and Niemeier (2002), Silvas (2015), Silvas et al. (2016). A new driving cycle is then built from chosen snippets assuming the Markov property, whose validity has also been demonstrated theoretically by Shi et al. (2013). In particular, two and three-dimensional Markov chains have been proposed by Silvas (2015), Silvas et al. (2016). More recently, Liu et al. (2020) extended this approach by considering variable passenger loads in the synthesis of driving cycles for city buses.

However, with a few exceptions, all the above approaches have been mainly applied to synthesising a single driving cycle starting from a large available dataset of road missions. By contrast, to reproduce variation in transport operations, it is necessary to dispose of a large number of driving cycles. These should ideally be constructed so that they are statistically equivalent or produce a meaningful spread in performance. A similar idea has been explored in Kivekas et al. (2018), Kivekas et al. (2017), where a procedure has been proposed for generating several driving cycles starting from a single bus route. The investigation was conducted with reference to number of stops Kivekas et al. (2018) and variable passenger load Kivekas et al. (2017). Both factors were shown to have a significant influence over energy consumption, which appeared to be almost normally distributed. To cope with the inherent uncertainties of driving cycles, Vepsalainen et al. (2018) also developed a simulation model to predict the energy demand of electric city buses. Variation in external settings like temperature and rolling resistance was modelled in Vepsalainen et al. (2018) adding extensive noise to an assumed nominal value.

At this point, there are two main arguments which may be raised against these conventional driving cycles. The first is that their pathological nature makes them inadequate for comparing different vehicles. By "pathological", the authors mean that an implicit correlation exists between the reference vehicle and the speed profile. Another demerit point is that, when a driving cycle is recorded, all the external effects (due to, say, traffic or wind conditions) are automatically incorporated. This is done implicitly, meaning that their influence cannot be understood or examined. Thus, the authors would then argue intuitively that a general, reliable representation of the environment should be independent of both vehicle and driver.

Following this principle, an antipodal description to the driving cycle has recently been proposed by Pettersson (2019), Pettersson

et al. (2019), Pettersson et al. (2019), Pettersson et al. (2020) and formalised in the so-called operating cycle (OC). This OC representation is not based on the concept of driving cycle and therefore no speed profile needs to be prescribed as input to the longitudinal vehicle model. On the contrary, the properties of both the mission and the external surroundings are modelled separately. A driver model is then used to dynamically translate the external stimuli into a desired speed. This circumvents the need to incorporate the information coming from the surroundings into the speed profile, since the OC is totally independent of both driver and vehicle.

In the OC representation, each physical quantity can be described via deterministic or statistical models. More specifically, the stochastic operating cycle (sOC) is conceived as a high-level representation of a transport mission and incorporates all the random parameters used to capture the statistical properties of a variable. On the other hand, the deterministic operating cycle (dOC) can be seen as a single realisation of an sOC and represents a low-level description of the environment in which the vehicle operates.

### 1.2. Contribution of this paper

Thus far, the modelling of the statistical parameters of the sOC has been limited to the road properties (for an exhaustive treatment, the reader is also referred to Johannesson et al. (2016), Johannesson et al.(2017)). However, weather and traffic conditions are also expected to play a crucial role in determining a vehicle's overall performance Donkers et al. (2020). For example, the local wind may favour or oppose the longitudinal motion of a truck, resulting in increased or diminished fuel consumption and emissions. Precipitation is also responsible for considerable reductions in vehicular speed (Akin et al., 2011; Hooper et al., 2013). On the other hand, traffic variables such as flow and density may contribute to the choice of the desired speed for the driver. Hence, the scope of this paper is to extend the OC representation to include stochastic weather and traffic parameters. In accordance with the principle of parsimony, these are conceived as mutually independent. This allows construction of a modular framework in which virtual prototypes can be tested and evaluated. It should be noted that the stochastic models for weather and traffic do not constitute a novelty when considered in isolation, since a great deal of research has been already lavished on dedicated studies. On the other hand, statistical modelling of weather and traffic is rarely attempted when describing road operations. The main contribution of the present work resides in its enhanced OC framework which collects new stochastic models for both categories. These models do contain information on typical conditions which take place during a transport mission, and allow for an intuitive representation of the driving environment. Furthermore, they can serve as statistical descriptors to offer more detailed prediction of usage variations. Unlike classic methods, this enables a more exhaustive representation of a transport operation, since vehicular performance can be evaluated and described by using different measures such as mean, variance ecc. Indeed, the focus of the OC representation is on modelling the surroundings rather than the vehicle's speed. This makes it possible to investigate the relationships existing between any performance index and a given set of parameters describing the environment, without the need for a reference, or *representative*, speed profile.

The second goal of this paper, therefore, is to illustrate the potential of the enhanced sOC format. To this extent, the natural process which enables a complete description of the transport environment using the OC representation is illustrated in detail. A method of data synthesis which can be used practically in vehicle design is proposed and implemented in MATLAB/Simulink® environment.

As an example of application, a fully parametrised sOC framewok, integrated with complete models for the driver and the vehicle, has been simulated in a virtual environment. This predicts the spread in $CO_2$ emissions resulting from different combinations of settings (with reference to weather and traffic scenarios). The study was conducted by means of a regression analysis in which the main influencing parameters were treated as categorical variables.

The structure of this paper is as follows: Section 2 discusses the salient features of the operating cycle description, plus its underlying principles. The novel stochastic models for both the weather and traffic categories are introduced in 3. Section 4 implements the parametrisation and the procedure for generating synthetic dOCs starting from a single sOC. The practical implementation of the OC format in a virtual simulation environment is also discussed, and detailed models for both driver and vehicle are introduced. The sensitivity analysis to quantify the impact of weather and traffic on $CO_2$ emissions is conducted in Section 5, where seasonality and traffic density are treated as categorical variables. Section 6 is dedicated to a general discussion on the limitation of the OC format in its current formulation, with some possible directions for future research. Finally, Section 7 summarises the conclusions.

## 2. Operating cycle descriptions

The scope of this paper is to extend the sOC initiated by Pettersson (2019), Pettersson et al. (2019) to include traffic and weather elements. The aim is to construct a stochastic model for all the factors which significantly impact vehicle performance in terms of $CO_2$ emissions and fuel consumption. These models must be built starting from physical principles and equations, ensuring that the parameters are relevant, understandable and measurable. This also simplifies the parametrisation from real data.

In deriving a set of desirable features to include in the model, one may begin by formulating a simple model of longitudinal vehicle dynamics in accordance with Newton's Second Law Wong (2008), Pacejka (2012), Heywood (1988), Guzzella and Sciarretta (2013), Mastinu and Ploechl (2014), Guiggiani (2018)):

$$m^* \dot{v}_x = F_x - F_{\text{grade}} - F_{\text{roll}} - F_{\text{air}}, \tag{1}$$

where $m^* = m + J_\text{w}/R_\text{w}^2$ is given by the total mass of the vehicle plus the sum of the reduced rotational inertias $J_\text{w}$, $R_\text{w}$ is the wheel radius, $v_x$ its longitudinal speed, $F_x$ the total longitudinal force acting in the tyre contact patches, $F_{\text{grade}}$ is the longitudinal projection of the gravitational force in the vehicle reference frame, $F_{\text{roll}}$ is the rolling resistance and $F_{\text{air}}$ the drag force. The resistive forces appearing in Eq. (1) read specifically:

**Table 1**

Stochastic (secondary) models and deterministic parameters (dOC parameters) for the sOC and dOC representations. *Linear* and *constant* refer to linear and right-side continuous piecewise constant interpolation models respectively. The mathematical model of *Dirac delta* occurs when the parameter is regarded as an isolated *event*.

| Model or parameter | Category | Type (for dOC) | Interp. model (for dOC) | Dim | Quantity |
|---|---|---|---|---|---|
| Speed signs | Road | Function | Constant | 1 | Speed limit |
| Altitude | Road | Function | Linear | 1 | Vertical coordinate |
| Curvature | Road | Function | Linear | 1 | Curvature |
| Ground type | Road | Function | Constant | 2 | Surface type, cone index |
| Roughness | Road | Function | Constant | 2 | Waviness, roughness coeff. |
| Stop signs | Road | Event | Dirac delta | 1 | Standstill time |
| Traffic lights | Road | Event | Dirac delta | 1 | Standstill time |
| Give way signs | Road | Event | Dirac delta | 1 | Standstill time |
| Speed bumps | Road | Event | Dirac delta | 3 | Length, height, angle of approach |
| Longitude | Road | Function | Linear | 1 | WGS84 longitude |
| Latitude | Road | Function | Linear | 1 | WGS84 latitude |
| Ambient temperature | Weather | Function | Linear | 1 | Temperature |
| Atmospheric pressure | Weather | Function | Linear | 1 | Pressure |
| Precipitation | Weather | Function | Constant | 1 | Precipitation amount |
| Wind velocity | Weather | Function | Constant | 2 | Velocity vector |
| Relative humidity | Weather | Function | Linear | 1 | Humidity |
| Traffic density | Traffic | Function | Constant | 1 | Density |
| Mission stops | Mission | Event | Dirac delta | 1 | Standstill time |
| Cargo weight | Mission | Function, event | Linear, constant | 1 | Payload |
| Power take-off | Mission | Function | Linear | 1 | Output power |
| Charging power | Mission | Function | Constant | 1 | Input power |
| Travel direction | Mission | Function | Constant | 1 | Driving direction |

$$F_{\text{grade}} = -mg\sin\alpha, \tag{2a}$$

$$F_{\text{roll}} = f_r mg\cos\alpha, \tag{2b}$$

$$F_{\text{air}} = \frac{1}{2}\rho_{\text{air}} C_d A \mid v_x^{\text{rel}} \mid v_x^{\text{rel}}, \tag{2c}$$

where $\alpha$ is the road slope angle defined according to ISO 8855, $f_r$ is the rolling resistance coefficient, $\rho_{\text{air}}$ the air density, $C_d$ the drag coefficient, $A$ the effective frontal area and $v_x^{\text{rel}}$ is the relative speed between the vehicle and the wind.

Accordingly, when the tyre slip losses are negligibly small, the requested power to propel the vehicle can be approximated by

$$P_{\text{drive}} = v_x \left( F_{\text{grade}} + F_{\text{roll}} + F_{\text{air}} - F_{\text{inertia}} \right), \tag{3}$$

with $F_{\text{inertia}} = -m^* \dot{v}_x$. Additionally, some extra amount of power might be required for external equipment, in which case the total power $P_{\text{tot}}$ produced from the energy source is

$$P_{\text{tot}} = P_{\text{drive}} + P_{\text{PTO}}. \tag{4}$$

Eq. (4) can be related to the instantaneous $CO_2$ emission rate (measured in mass per unit of time, for instance). The right hand side in Eq. (4) is the requested power. This depends on the operational environment and owner utilisation but does not on the vehicle powertrain. Therefore, a statistical description of the right-hand side of Eq. (4) is useful in understanding how the energy usage varies for a vehicle design choice.

In the following, this paper will consider only those external variables which may affect vehicle performance and which may be deduced directly by looking at the specific nature of the contributions showing up in (1) or via a driver model. To better understand the candidate physical quantities to be included in the model, the terms appearing in (1) may be rewritten in extended form:

- $F_{\text{inertia}} = -m^* \dot{v}_x$. This term is proportional to the acceleration. Thus, any factor which may contribute to the vehicle changing its speed dynamically is implicitly included. Depending on the traffic and weather conditions, a driver may choose the desired speed based on the following quantities: traffic density, precipitation and asphalt properties.
- $F_{\text{grade}} = -mg\sin\alpha$. The slope angle $\alpha$ is often described as a road gradient measured as a percentage. This is a road parameter and an exhaustive description may be found in Pettersson (2019), Pettersson et al. (2019).

- $F_{\text{roll}} = f_r mg\cos\alpha$. This equation empirically models the energy loss due to viscoelastic properties of the tyre in its interaction with the road surface[3]. The rolling resistance coefficient $f_r$ depends on the road properties, ground type and weather conditions.
- $F_{\text{air}} = \rho_{\text{air}} C_d A |v_x^{\text{rel}}| v_x^{\text{rel}}/2$. In this equation, there are different physical quantities which need to be properly considered. The first noteworthy thing is that the speed in question is the relative one between vehicle and wind. Hence, a wind model is needed. Furthermore, the air density $\rho_{\text{air}}$ is a function of the air pressure $p_{\text{air}}$ and temperature $T_{\text{air}}$. The simplest model which accounts for this interaction is that of an ideal gas:

$$\rho_{\text{air}} = \frac{p_{\text{air}}}{RT_{\text{air}}}. \tag{5}$$

Eq. (5) justifies the necessity of detailed models for the air temperature and pressure. As secondary effects, the external temperature might influence a combustion engine's efficiency, but such complex phenomena are not modelled in this paper.

The operating cycle (OC) is a mathematical description of a road transport mission which includes all the relevant features from the surroundings and is independent of both vehicle and driver models. To be more precise, the OC framework comprises two main levels of representation.

The first, called the deterministic operating cycle (dOC), describes the mission and external environment with high accuracy. Four different categories are defined: road, traffic, weather and mission. A different set of parameters is used for each of them. More specifically, a generic parameter, corresponding to a physical quantity, is defined as discrete function of time and position. Some parameters are only made dependent on either the position or the time. Some others, like the ones marked in the traffic category, depend on both. Additionally each parameter may be represented by a scalar or vector-valued signal (see dimensionality in Table 1). Any value in between two different discrete times (or positions) may be computed by interpolation using the corresponding model in Table 1. To formalise the dOC format mathematically, the four categories (see Table 1) may be defined as the sets containing the parameter sequences: $\mathscr{R}_d$ is the set containing all sequences labelled as road, $\mathscr{W}_d$ for weather, $\mathscr{T}_d$ for traffic and $\mathscr{M}_d$ for mission. The subscript stands for *deterministic*. The dOC format may then be formally defined as the collection of sets:

$$\mathscr{OC}_d = \{\mathscr{R}_d, \mathscr{W}_d, \mathscr{T}_d, \mathscr{M}_d\}, \tag{6}$$

and interpolation may be defined as an operator acting on the elements in the sets. The dOC format provides a detailed view of individual transport operations without making any assumptions about the driver or vehicle. Furthermore, it is built in a modular fashion such that parameters may easily be modified, added or removed.

The second type of representation, called the stochastic operating cycle (sOC), is less detailed. It consists of a statistical description of both the external environment and mission characteristics. In the sOC, the dOC parameters become sOC models, and more specifically *secondary models*, as better explained in Section 3. Analogous to the dOC parameters, the sOC models are, in turn, grouped into the same four categories: road, traffic, weather and mission. Furthermore, each sOC model is provided with its own set of sOC parameters, denoted by $\mathscr{OC}_s$. These are chosen so as to capture the relevant statistical properties (mean, variance, and so on) of a quantity and may be themselves related to physical entities, but their interpretation is not always straightforward. The structure of the sOC is conceived as simply as possible and the models are thought to be independent of each other. Formally, the set of sOC parameters may be defined as:

$$\mathscr{OC}_s = \{\mathscr{R}_s, \mathscr{W}_s, \mathscr{T}_s, \mathscr{M}_s\}, \tag{7}$$

where this time $\mathscr{R}_s, \mathscr{W}_s, \mathscr{T}_s$ and $\mathscr{W}_s$ are the sets containing all the sOC parameters, marked respectively as road, weather, traffic and mission, and the subscript stands for *stochastic*. It is worth remarking that a complete collection of models and parameters for the road category has already been developed fully in Pettersson et al. (2019). In this paper, the focus is on the traffic and weather categories.

Naturally, there is a correlation between the two levels of representation. In fact, it is always possible to relate each description to the other one. Indeed, given a set of stochastic parameters, a dOC may be interpreted as a single realisation of an sOC. Two dOCs originating from the same sOC are thus equivalent in a statistical sense, but may differ significantly in practice. This also implies that the map between an sOC and a dOC is not necessarily bijective; quite the opposite. This aspect will be clarified later on in Section 5 through a concrete example. On the other hand, given a dOC, it is possible to estimate the corresponding stochastic parameters and hence obtain an equivalent description in terms of an sOC.

## 3. The stochastic operating cycle

A stochastic model may be used to measure and mathematically reproduce variation in a transport operation. Many of the approaches found in the scientific literature dealing with uncertainty and variation of $CO_2$ emissions utilise stochastic processes Ashatari et al. (2014), Lee and Filipi (2011), Asbogaard et al. (2007). In contrast to the above works, which focus on driving cycles, this study needs to account for the operating cycle properties when using stochastic processes Pettersson (2019). As already mentioned, the sOC representation is conceived to be a mid-level description of a transport operation, and may serve as basis for generating synthetic dOCs.

---

[3] For an exhaustive treatment of analytical tyre models, the reader is referred to such works as Pacejka (2012, Guiggiani (2018)), Romano et al. (2020b), Romano et al. (2020a).
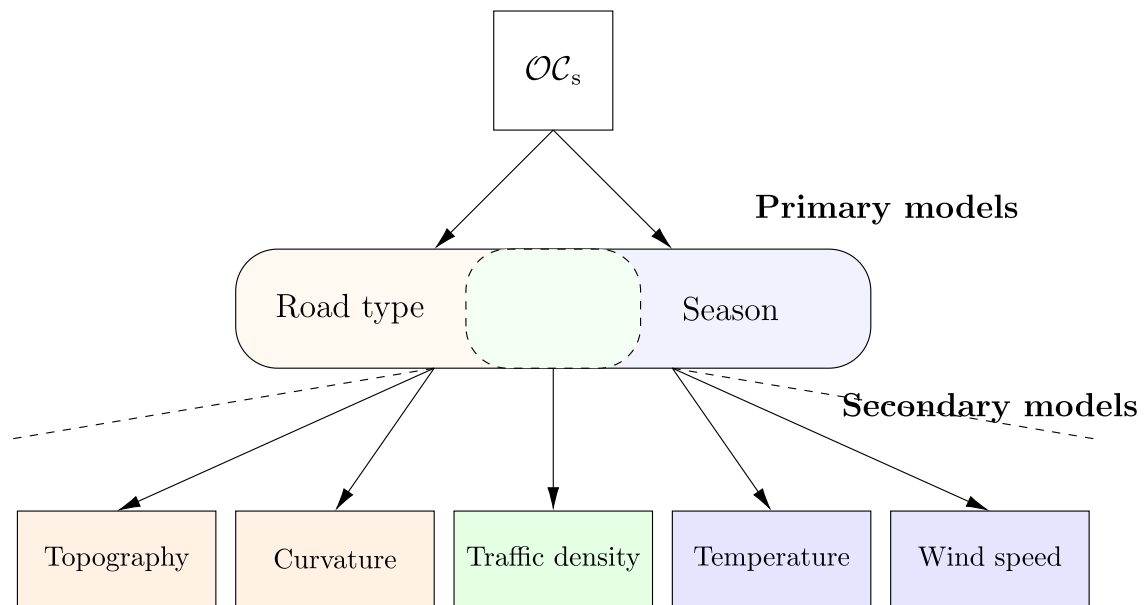
**Fig. 1.** Hierarchical structure of an sOC. Both the road type and season are primary models and influence the value of the statistical parameters for the secondary models. Whilst the (secondary) road and weather parameters depend only on the respective primary model, the traffic ones are simultaneously determined by the road type and season.

This concept was introduced for the first time in Pettersson et al. (2019). At the time, the format only included stochastic models for the road parameters listed in Table 1, whilst suitable models for the other categories had not yet been formulated. The version of sOC presented in this paper consists instead of a complete statistical description of a transport mission, and integrates the existing models for the road with novel ones for the traffic and weather categories. The golden rule illustrating the essence of the sOC format is the parsimony principle. The framework is built with the philosophy of being as simple as possible. This means that complicated multi-variate distributions are avoided, thus requiring each individual model to be treated as a separate entity[4]. The latter assumption is quite strong (if questionable) but, in practical terms, simplifies the stochastic description enormously. At the same time, it guarantees modularity and allows for ease of implementation. Clearly, even in this case, the interaction between the sOC parameters should be preserved, or the format would eventually result in a poor representation. This may be circumvented by arranging the actual operating cycle in a hierarchical fashion, as outlined in Pettersson et al. (2019). In this way, it is possible to achieve a modular structure equipped with a high level of diversification. The (main) obvious disadvantage is that the hierarchical ordering unavoidably increases the effective number of values needed for each parameter.

### 3.1. Primary models

In the sOC format, the balance between complexity and realism is achieved by defining two separate set of models: primary and secondary ones. In Pettersson et al. (2019), in which only the road category was considered, the hierarchical ordering was obtained by distinguishing between different road types. The subordinate (secondary) road models then inherited a different set of sOC parameters for each road type. The same reasoning is followed in this paper, but an additional primary model for the weather category is introduced: seasonality. Thus, the primary models become the road type (variable in numbers depending on the specific geographical location) and season. No primary model for the traffic and mission categories is proposed.

The secondary models for the road and weather are then treated separately; these should only derive their set of sOC parameters from the corresponding primary model. This implies, for example, that the values of sOC parameters for curviness are not affected by the season. Analogously, the sOC parameters for the air temperature completely ignore any dependency on the road type, such as urban, rural and so on. By contrast, the traffic model is more complex and deserves an explanation. Initially, it would seem natural to presume that the traffic properties depend on the specific road type; this is quite intuitive. Traffic conditions taking place in urban areas are likely to be completely different from those on highways or in rural zones. At the same time, periodic trends in traffic flow and density may be identified on both daily and seasonal scales. Therefore, it is necessary to account for variations in time. This may be done by assuming a correlation between the traffic scenario and the season. Hence, the authors propose to use only a secondary model for traffic; this inherits its own set of sOC parameters from the primary road and weather models. Fig. 1 illustrates the resulting composite edifice, with the interaction between primary and secondary models.

---

[4] Basically, mutual dependencies between the sOC models are systematically neglected.

Sections 3.2 and 3.3 introduce and discuss the secondary models for weather and traffic.

### 3.2. Secondary weather models

The *secondary weather models* introduced in this paper are ambient temperature, atmospheric pressure, wind velocity and relative humidity.

#### 3.2.1. Air temperature and relative humidity

Some weather parameters, such as air temperature and relative humidity, exhibit seasonal trends which are deterministic in nature Liu et al. (2018), Eymen and Koylii (2019) and relatively easy to model intuitively. Therefore, for both physical quantities, whose sequences are denoted by $\{T_{air,k}\}$ and $\{\Psi_{RH,k}\}$ respectively, a distinction is made between a deterministic component (which tries to capture the diurnal and seasonal trends) and a stochastic one (to replicate random variations which may occur during the day). The complete models are thus assumed to be of the form:

$$T_{air,k} = \mu_T + T_d \sin\left(\omega_d d_d[t] + \varphi_{T_d}\right) + T_y \sin\left(\omega_y d_y[t] + \varphi_{T_y}\right) + \widetilde{T}_k, \tag{8}$$

$$\Psi_{RH,k} = \mu_\Psi + \Psi_d \sin\left(\omega_d d_d[t] + \varphi_{\Psi_d}\right) + \Psi_y \sin\left(\omega_y d_y[t] + \varphi_{\Psi_y}\right) + \widetilde{\Psi}_k, \tag{9}$$

where $\omega_d = 2\pi/24$ and $\omega_y = 2\pi/365$ are the daily and annual frequencies of the periodic signal, and $d_d[t]$ and $d_y[t]$ are the daily mod and annual ceiling operators (Liu et al., 2018), defined respectively as

$$d_d[t] = (t \bmod 24), \tag{10a}$$

$$d_y[t] = \left\lceil \frac{t}{24} \right\rceil. \tag{10b}$$

In Eq. (8), the quantities $\mu_T$ and $\mu_\Psi$ represent the average temperature and humidity over the year; the amplitudes $T_d, T_y$ and $\Psi_d, \Psi_y$ model the daily and annual deterministic trends, whilst the random variables $\widetilde{T}_k$ and $\widetilde{\Psi}_k$ capture residuals (Box et al., 2015). More specifically, a simple AR(1) process is used to model the stochastic components as follows:

$$\widetilde{T}_k = \phi_T \widetilde{T}_{k-1} + e_{T,k}, \qquad e_{T,k} \sim \mathcal{N}\left(0, \sigma_{e_T}^2\right), \tag{11}$$

$$\widetilde{\Psi}_k = \phi_\Psi \widetilde{\Psi}_{k-1} + e_{\Psi,k}, \qquad e_{\Psi,k} \sim \mathcal{N}\left(0, \sigma_{e_\Psi}^2\right), \tag{12}$$

where the characteristic parameters are $\phi_T, \sigma_{e_T}^2$ and $\phi_\Psi, \sigma_{e_\Psi}^2$.

It is worth pointing out that the deterministic components for both models are calculated over the total year, and therefore the parameters $\mu_T, \mu_\Psi, T_d, T_d, \Psi_d, \Psi_y, \varphi_{T_d}, \varphi_{T_y}$ and $\varphi_{\Psi_d}, \varphi_{\Psi_y}$ are independent of the seasonal setting. Conversely, the stochastic parameters $\phi_T, \phi_\Psi, \sigma_{e_T}^2$ and $\sigma_{e_\Psi}^2$ inherit their values from the specific season, which is the primary weather model.

#### 3.2.2. Atmospheric pressure

For the atmospheric pressure parameter $p_{air}$, the seasonal frequencies are not easily interpretable and, therefore, a modelling approach like that used in Section 3.2.1 may not be the most appropriate. Rocca et al. (2010) have shown that the atmospheric pressure trend may be foreseen by using gaussian ARIMA$(p, d, q)$ processes. In other words, autoregressive models with moving average[5], with $p$ standing for the order of the autoregressive model (AR), $d$ for the number of differencing, and $q$ for the order of the moving-average (MA) model. Basically, ARIMA$(p, d, q)$ models generalise an AR$(p)$ autoregressive process by adding dependence on previous errors and states. Using the lag operator notation, it may be sintetically written:

$$\phi_P\left(L\right)(1 - L)^d P_{air,k} = c_P + \theta_P\left(L\right) e_{P,k}, \qquad e_{P,k} \sim \mathcal{N}\left(0, \sigma_{e_P}^2\right), \tag{13}$$

where $\phi_P(L)$ is a stable degree $p$ AR lag operator polynomial and $\theta_P(L)$ is an invertible degree $q$ MA operator polynomial. To summarise, the model for atmospheric pressure is fully parametrised by the constant term $c_P$, the autoregressive coefficients $\phi_{Pj}, j = 1, \ldots, p$, the moving average coefficients $\theta_{Pi}, i = 1, \ldots, q$ and the innovation variance $\sigma_{e_P}^2$.

#### 3.2.3. Precipitation occurrence and amount

The sequence for atmospheric precipitation is modelled in a two-step process. In the first step, the occurrence of the event $\{H_{p,k}\}$ is simulated, and then a suitable probability distribution is used to fit the intensity $\{\Lambda_{p,k}\}$, which corresponds to the precipitation amount. The occurrence is modelled by using a Markov chain of fixed interval length, similar to what was done in Gabriel and Neumann (1962),

---

[5] For additional information, the reader is again redirected to Bowerman and O'Connel (2004), Box et al. (2015).

Chin (1977). The stochastic variable $H_{p,k}$ is allowed to take states from the finite space $\{1,2\}$, where 1 and 2 are the respective labels for the *dry* and *wet* events. The main assumption is that the probability of the event occurring at the discrete time $k$ depends only on the previous occurrence at the time $k-1$. The intensity of the phenomenon plays no role in this process. Therefore, the probability of the event occurrence may be approximated as follows:

$$
\begin{aligned}
&\mathbb{P}\big(H_{p,k} = h_{p,k}\big|H_{p,1} = h_{p,1}, H_{p,2} = h_{p,2}, \ldots, H_{p,k-1} = h_{p,k-1}\big) \\
&\approx \mathbb{P}\big(H_{p,k} = h_{p,k}\big|H_{p,k-1} = h_{p,k-1}\big).
\end{aligned}
\tag{14}
$$

This is called a Markov property, and implies that the sequence may be modelled using a Markov chain (the reader is referred to such works as Hsu (2020) for an introduction on the topic). The Markov process (14) is fully characterised by a transition matrix $\mathbf{P}_H \in \mathbb{R}^{2\times 2}$, whose dimension depends on the number of possible states $n_H = 2$. An entry $p_{Hij}$ of the matrix $\mathbf{P}$ describes the transition probability from the state $i$ to $j$ and satisfies:

$$
\sum_j p_{Hij} = 1.
\tag{15}
$$

For the case under consideration there are only two states, and hence the two following conditions hold:

$$
p_{H12} = 1 - p_{H11},
\tag{16a}
$$

$$
p_{H21} = 1 - p_{H22}.
\tag{16b}
$$

Thus, only the transition probabilities $p_{H11}$ and $p_{H22}$ need to be estimated. The estimation can be carried out considering the two ratios

$$
p_{H11} = f_{H11}/(f_{H11} + f_{H12}),
\tag{17a}
$$

$$
p_{H22} = f_{H22}/(f_{H21} + f_{H22}),
\tag{17b}
$$

The interpretation in physical terms of the coefficients $f_{Hij}$ appearing in Eqs. (17) is quite straightforward. For example, the coefficient $f_{H11}$ represents the number of dry intervals preceded by dry intervals, whilst $f_{H12}$ is the number of wet intervals preceded by dry ones. Therefore, the coefficients $f_{Hij}$ are used to parametrise the precipitation occurrence, as they are easier to understand.

Once that the Markov parameters have been derived, a suitable distribution is required to model the intensity of the event. Traditionally, the amount of precipitation is modelled using Weibull or Gamma distributions Husak et al. (2007), Kumar et al. (2017), as these appear to capture the monthly and seasonal trends quite well. This paper proposes a Gamma distribution and thus, at each discrete time $k$, the formula is

$$
\Lambda_{p,k} \sim \mathrm{Ga}\big(\alpha_{\Lambda_p}, \beta_{\Lambda_p}\big).
\tag{18}
$$

where the PDF of the Gamma distribution with generic shape and rate parameters $\alpha$ and $\beta$ is given by

$$
f\bigg(x; \alpha, \beta\bigg) = \frac{\beta^\alpha x^{\alpha-1} e^{-\beta x}}{\Gamma(\alpha)}, \qquad x > 0, \quad \alpha, \beta > 0.
\tag{19}
$$

in which $\Gamma(\cdot)$ is the gamma function.

Hence, the precipitation model is fully described by the coefficients $f_{Hij}$ and the shape and rate parameters $\alpha_{\Lambda_p}$ and $\beta_{\Lambda_p}$.

### 3.2.4. Wind speed and direction

Different approaches to wind modelling have been proposed in the literature, including hybrid and complex multivariate formulations Hocaoglu et al. (2010), Cadenas et al. (2016). The main complication when dealing with this parameter is that wind speed and direction often exhibit a strong correlation. Hence, the two signals need to be modelled properly by taking into account their mutual interaction. A natural (and simple) possibility is to resort to a VAR model, which extends the standard notion of an autoregressive series by coupling different random processes. This may be notated thus:

$$
\mathbf{\Phi}_w(L) Y_{w,k} = \boldsymbol{c}_w + \boldsymbol{e}_{w,k},
\tag{20}
$$

where the vector $Y_{w,k} = \begin{bmatrix} V_{w,k} & \Theta_{w,k} \end{bmatrix}^{\mathsf{T}}$ collects the wind speed $V_{w,k}$ and direction $\Theta_{w,k}$ at each discrete time step $k$, the parameter $\boldsymbol{c}_w \in \mathbb{R}^2$ represents a constant offset and $\boldsymbol{e}_{w,k} \in \mathbb{R}^2$ is the vector of normally distributed innovations with covariance matrix given by $\boldsymbol{\Sigma}_{\boldsymbol{e}_w} \in \mathbb{R}^{2\times 2}$. Finally, the matrix operator $\mathbf{\Phi}_w(L)$ reads

$$
\mathbf{\Phi}_w\bigg(L\bigg) = \mathbf{I} - \sum_{j=1}^{p} \mathbf{\Phi}_{wj} L^j,
\tag{21}
$$

in which every $\mathbf{\Phi}_{wj} \in \mathbb{R}^{2\times 2}$ is a matrix of AR coefficients. An intermediate step is needed for the wind direction, which is a circular variable. This is preliminarily converted into a linear variable by using the inverse of the link function as follows:
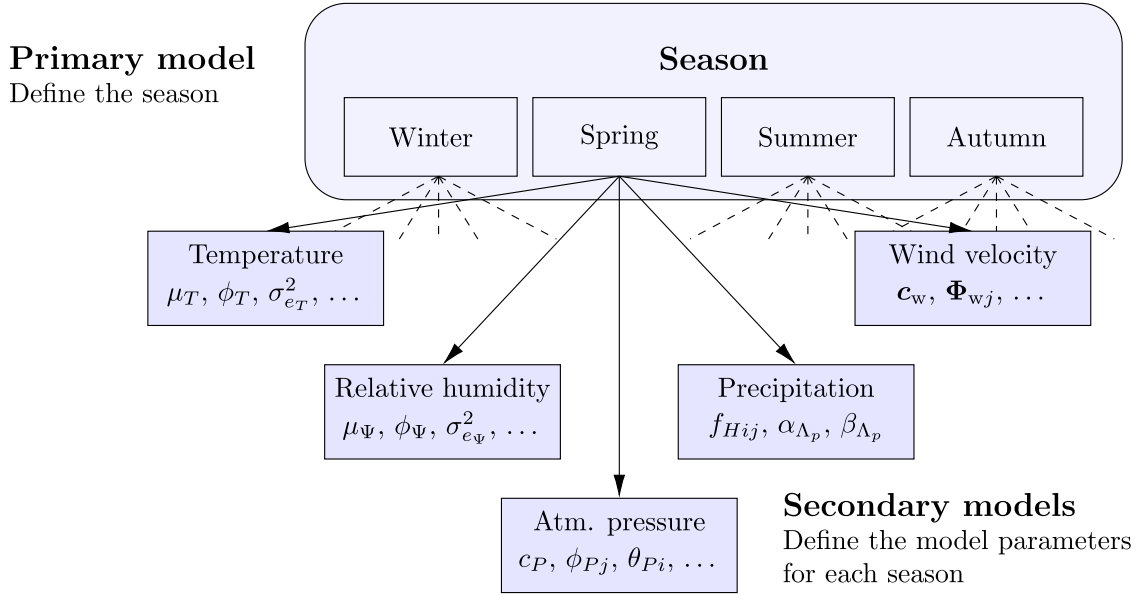
# Primary model

Define the season



**Fig. 2.** The season is the primary weather model. The other parameters are treated as ancillary and inherit their values depending on the season.

$$g\left(\Theta_{\mathrm{w}}\right) = 2\pi\left(\Phi\left(\Theta_{\mathrm{w}}\right) - \frac{1}{2}\right) + \mu_{\Theta_{\mathrm{w}}}, \tag{22}$$

in which $\mu_{\Theta_{\mathrm{w}}}$ represents the mean wind direction and $\Phi(\cdot)$ is the cumulative distribution function for standardised Gaussian distribution with mean and variance of 0 and 1, respectively. The inverse of Eq. (22) is computed by

$$g^{-1}\left(\Theta_{\mathrm{w}}\right) = \Phi^{-1}\left(\frac{(\Theta_{\mathrm{w}}) - \mu_{\Theta_{\mathrm{w}}}}{2\pi} + \frac{1}{2}\right), \tag{23}$$

where $\Phi^{-1}(\cdot)$ is called a probit function. Using Eq. (23), the wind direction is firstly converted into a linear variable, and the VAR process is than applied for forecasting. The variable is then converted to the circular form again by applying Eq. (22). Further details are given in Erdem and Shi (2011), Fisher (1993). In summary, the wind model is fully described by the average direction $\mu_{\Theta_{\mathrm{w}}}$, the constant term $\boldsymbol{c}_{\mathrm{w}}$, the error covariance matrix $\boldsymbol{\Sigma}_{e_{\mathrm{w}}}$ and the autoregressive matrices $\boldsymbol{\Phi}_{\mathrm{w}j}, j = 1, \dots, p$. A graphical illustration of the hierarchical structure of the secondary weather models is shown in Fig. 2.

## 3.3. Secondary traffic model

Average characteristics of vehicular traffic are important when it comes to assessing energy efficiency Sciarretta (2020). The customary approach consists of describing traffic using macroscopic variables. The three main variables to consider are the traffic density $\rho_{\mathrm{t}}(x,t)$, expressed as a number of vehicles per distance, the traffic speed $v_{\mathrm{t}}(x,t)$, and the traffic flow $q_{\mathrm{t}}(x,t) = \rho_{\mathrm{t}}(x,t)v_{\mathrm{t}}(x,t)$, usually measured in number of vehicles per unit of time.

In both the dOC and the sOC formats, the traffic density $\rho_{\mathrm{t}}$ is the only parameter indicated[6], and hence only one model is needed for traffic. Specifically, like air temperature and humidity, the traffic density is characterised by a deterministic diurnal component. Thus, for each combination of road type, speed sign and season, the traffic density is modelled as follows:

$$\rho_{\mathrm{t},k} = \mu_\rho + \rho_{\mathrm{d}}\sin\left(\omega_{\mathrm{d}}d_{\mathrm{d}}[t] + \varphi_{\rho_{\mathrm{d}}}\right) + \widetilde{\rho}_k, \tag{24}$$

where $\mu_\rho$ is the average density on a specific road segment during the season, $\rho_{\mathrm{d}}$ is the amplitude of the daily variation, $\omega_{\mathrm{d}} = 2\pi/24$ is again the daily frequency, $\varphi_{\rho_{\mathrm{d}}}$ the initial phase and $\widetilde{\rho}_k$ represents the stochastic component. For the sake of simplicity, the latter has again been captured using an AR(1) process:

$$\widetilde{\rho}_k = \phi_\rho\widetilde{\rho}_{k-1} + e_{\rho,k}, \qquad e_{\rho,k} \sim \mathcal{N}\left(0, \sigma_{e_\rho}^2\right). \tag{25}$$

Once a stochastic model for the traffic density has been established, it is also necessary to relate it to the desired speed input for the

---

[6] As explained below, assuming stationary flow, density, speed and flow are correlated.

**Table 2**
Summary of sOC parameters for weather and traffic models.

| Model | Model type | No. of states | No. of parameters | Symbol |
|---|---|---|---|---|
| Temperature | Deterministic | Continuous | 5 | $\mu_T, T_d, T_y, \varphi_{T_d}, \varphi_{T_y}$ |
| | Gaussian AR(1) | Continuous | 2 | $\phi_T, \sigma_{e_T}^2$ |
| Relative | Deterministic | Continuous | 5 | $\mu_\Psi, \Psi_d, \Psi_y, \varphi_{\Psi_d}, \varphi_{\Psi_y}$ |
| humidity | Gaussian AR(1) | Continuous | 2 | $\phi_\Psi, \sigma_{e_\Psi}^2$ |
| Atmospheric | Gaussian ARIMA$(p, d, q)$ | Continuous | $2 + p + q$ | $c_P, \phi_{Pj}, \theta_{Pi}, \sigma_{e_P}^2$ |
| pressure | | | | |
| Precipitation | Markov process | 2 | 4 | $f_{Hij}$ |
| | Gamma distributed | – | 2 | $\alpha_{\Lambda_p}, \beta_{\Lambda_p}$ |
| Wind speed | Gaussain VAR$(p)$ | Continuous | $6 + 4p$ | $\mu_{\theta_w}, c_w, \boldsymbol{\Phi}_{wj}, \boldsymbol{\Sigma}_{e_w}$ |
| and direction | | | | |
| Traffic | Deterministic | Continuous | 5 | $\nu_f, \rho_c, \mu_\rho, \rho_d, \varphi_{\rho_d}$ |
| density | Gaussian AR(1) | Continuous | 2 | $\phi_\rho, \sigma_{e_\rho}^2$ |

driver, since the variable $\rho_t$ does not show explicitly in Eq. (1). Thus, this paper will assume the traffic to be stationary and homogeneous on each road segment between two discrete times. Accordingly, an equilibrium relationship between the traffic density and speed may be postulated in the form $v_t(x,t) = v_e(\rho_t(x,t)) = f(\rho_t(x,t))$. The relationship $v_e(\rho_t(x,t)) = f(\rho_t(x,t))$ constitutes the so-called fundamental diagram of the traffic flow and is specifically stated for a given type of road. In the literature, different possible models have been proposed to capture the dependency of the equilibrium speed on the traffic density; these have mostly been based on empirical fitting (see Kessels (2019) for an introduction). Consistent with the principle of parsimony, this paper uses the simplest possible model, known as Greenshield's fundamental diagram (see discussion in Section 4.1). In formula, it may be expressed as follows:

$$v_e(\rho_t(x,t)) = v_f\left(1 - \frac{\rho_t(x,t)}{\rho_c}\right), \tag{26}$$

where $v_f$ represents the *free-flow* speed, i.e. the traffic speed corresponding to have almost no vehicle on the road, and $\rho_c$ is the *critical density*. It may be observed that $v_e$ is a strictly decreasing function of the density according to Eq. (26). Furthermore, the value $\rho_t = \rho_c/2$ indicates the transition between the so-called *free-flow* traffic regime and the *congested* one, as may be also deduced by plotting the equilibrium flow $q_e(x,t) = v_e(\rho_t(x,t))\rho_t(x,t)$. In the OC format, both the quantities $v_e$ and $\rho_c$ depend on the specific road type (urban, rural, highway) and, in turn, on legal speed limit for each section. In any case, both $v_e$ and $\rho_c$ are presumed to be independent of the season.

The traffic density model is therefore described completely by the parameters $\mu_\rho, \rho_d, \varphi_{\rho_d}$ and $\sigma_{e_\rho}^2$, which are functions of both road type and season, plus the *fundamental* parameters $v_e$ and $\rho_c$, which only vary depending on the road properties.

The stochastic models for weather and traffic are finally summarised in Table 2,

## 4. Model implementation and simulation

To be useful in product development, an sOC must be translated into a deterministic representation. This may be done by generating synthetic dOCs whose parameters may be interpreted as a realisation of the corresponding stochastic models. Section 3 outlined the mathematical theory behind the OC description. This paper will now move on to explaining how an sOC can be successfully parametrised and converted into a (virtually infinite) number of equivalent deterministic operating cycles. These may, in turn, be used in a virtual environment to simulate a vehicle's behaviour, allowing for energy efficiency prediction, design optimisation and function development.

### 4.1. Model parametrisation

Starting from the road models, the parametrisation may be worked out based on vehicle data logged during transport operations. This is the same approach followed in Pettersson et al. (2019), from which the authors of this paper borrowed the road parameters for the subsequent examples. The overall procedure is not repeated here, as the scope of this work is only the weather and traffic categories. To be concise, based on a dataset available for the Jönköping area, it was possible to identify three road types: urban, rural and highways, each with its own set of speed limits (30 and 50 kph for urban roads, 60, 70 and 80 for rural ones and 90, 100 and 110 for highways). For more detailed information about the parameter values for the road category, the reader is again referred to Pettersson et al. (2019).

For the weather models, the simplest and most intuitive choice is to resort to external databases. An example is the Swedish

Meteorological and Hydrological Institute[7] (SMHI), which collects weather data throughout the year, at different stations located all over Sweden. This is particularly practical when it comes to analysing transport operations taking place within a well-defined geographical area, for which the weather parameters may be assumed to remain approximately constant. If the road missions extend into a larger area, an option is to build a weather map by combining information collected from multiple stations. To tune the models for this paper, the authors acquired data from the central Göteborg station[8], since the scope of this paper's example is mostly illustrative. The time resolution for each physical quantity was one hour, with the exception of the precipitation amount for which data was available every 15 min. Therefore, apart from the precipitation model, the discrete component of each model was parametrised on the same time scale.

From Table 2, it can be also deduced that the sOC models for atmospheric pressure and wind speed and direction leave a certain freedom choosing the values for the orders $p$ and $q$. For the specific case under consideration, with $p = 3, d = 0$ and $q = 0$, the model for atmospheric pressure was fully parametrised by the constant term $c_P$, the three autoregressive coefficients $\phi_{P1}, \phi_{P2}, \phi_{P3}$ and the variance $\sigma_{e_P}^2$. For the wind speed and direction, good agreement was found by setting $p = 2$. Hence, only two matrix lag operators, $\mathbf{\Phi}_{w1}$ and $\mathbf{\Phi}_{w2}$, were needed to describe the model completely. The values for the weather sOC parameters are listed in Table 3. Note that these values are not necessarily adequate for all datasets.

The sOC traffic model was parametrised using the same rationale. The authors' main source was the Trafikverket (the Swedish Transport Administration) database[9], collecting sparse traffic flow data (traffic flow and mean speed) which is free to download. The time resolution in this case was also one hour, but data was collected for a maximum of three consecutive days on the same section of road. To parametrise the model, the authors distinguished between road types and segments based on the legal speed limit, and clustered together data relating to the same combination. Since the structure of the traffic model is closely connected to that used for the road category[10], the chosen stations were those around the Jönköping area, for which road models had already been parametrised in Pettersson et al. (2019). The choice of Greenshield's relationship for the fundamental diagram was a pragmatic one and mainly justified by the parsimony principle. Indeed, no data capturing the lower part of the diagram was available. Thus, in the absence of satisfactory information, the simplest model was preferred.

Ultimately, the parametrised sOC resulting from this operation does not correspond to any specific setting, but is still complete and useful in various analyses. The sOC parameter values for the weather and traffic models (after the fitting procedure) are listed in Table 3.

## 4.2. Data synthesis

The second aspect concerns the generation of dOCs starting from the models that had already been parametrised. Fig. 3 is a schematic illustration of the typical workflow which synthesises a reference dOC starting from an equivalent sOC. First, the primary models are generated over a specified mission distance, which is prescribed by the user and subsequently included in the mission parameters. For each season, the starting time (day and hour) can be generated randomly or specified by the user. The number of days is another input to the process. This then simulates the weather and traffic time series over a finite horizon. The time resolution for this operation is the same as the one used to parametrise each sOC model. The primary models are also generated simultaneously, since no explicit interaction is expected between the two. It is worth mentioning that, whilst the overall road consists of a sequence of road types, the season is assumed to be constant over the mission. Both models are simulated depending on their stationary distribution, which is trivial for the weather category. The secondary sOC models are then derived from the primary ones. Quantities such as topography and curvature depend only on the road type. On the other hand, weather parameters like temperature, wind speed and direction are only affected by the season. The traffic time series may be only produced when the road has been completely modelled and the season determined. For the secondary models, the simulation of road properties may be carried out using the *ad hoc* WAFO package implemented in MATLAB®, whilst the weather models using the Econometric Toolbox. The sequences obtained using this procedure need to be converted into the dOC language. For example, curviness and topography are translated into road curvature $\kappa$ and altitude (or, equivalently, road grade $\alpha$); similarly, wind speed (in magnitude) and direction are instead reformulated in terms of velocity vector $\mathbf{v}_w$, where the components are specified. Furthermore, wind speed is usually measured at weather stations at approximately 10 m above the ground. Therefore, the value must be converted to ground level[11]. From the signed curvature, the actual road profile and the tangent vector to the trajectory are also deduced numerically using Fresnel integrals. This step is crucial since it allows computation of the relative direction between the vehicle and wind velocity vector, as discussed later in Section 5. The dOC parameters, plus their location in either space or time (or both for the traffic density), are finally encoded in the dOC description and tabulated.

A graphical example of the simulated road properties may be found in Pettersson et al. (2019). Related discussions are beyond the scope of the present paper and are omitted here. Instead, results for the weather and traffic categories with the stochastic parameters in Table 3 are shown in Fig. 4. The time horizon corresponds to a total of 10 winter days. The first quantity represented in blue is the

---

[7] https://www.smhi.se/en/weather/sweden-weather/observations#ws=wpt-a,proxy=wpt-a,tab=vader,param=t.

[8] Ironically, weather stations for the Jönköping area are lacking of data, whilst no data for the road category was available for Göteborg.

[9] https://vtf.trafikverket.se/SeTrafikinformation.

[10] The secondary weather parameters also exhibit dependency on seasonality, but not directly on the secondary weather parameters, as already explained in SubSection 3.3.

[11] In our case, using the logarithmic speed profile (Tennekes, 1973).

**Table 3**
sOC parameters for weather and traffic models models in Section 4.

### Weather models

| Model | Parameter | Value (per season) | | | | Unit |
|---|---|---|---|---|---|---|
| | | Winter | Spring | Summer | Autumn | |
| Temperature | $\mu_T$ | | | 9.52 | | °C |
| | $T_\mathrm{d}$ | | | 8.75 | | °C |
| | $T_\mathrm{y}$ | | | 1.53 | | °C |
| | $\varphi_{T_\mathrm{d}}$ | | | −2.11 | | rad |
| | $\varphi_{T_\mathrm{y}}$ | | | 3.15 | | rad |
| | $\phi_T$ | 1.379 | 1.252 | 1.254 | 1.373 | - |
| | $\sigma^2_{e_T}$ | 0.270 | 0.648 | 0.532 | 0.326 | °C$^2$ |
| Relative humidity | $\mu_\Psi$ | | | 77.13 | | % |
| | $\Psi_\mathrm{d}$ | | | 8.70 | | % |
| | $\Psi_\mathrm{y}$ | | | 5.94 | | % |
| | $\varphi_{\Psi_\mathrm{d}}$ | | | 1.719 | | rad |
| | $\varphi_{\Psi_\mathrm{y}}$ | | | 0.400 | | rad |
| | $\phi_\Psi$ | 1.188 | 1.167 | 1.120 | 1.146 | - |
| | $\sigma^2_{e_\Psi}$ | 8.079 | 22.266 | 23.470 | 12.851 | - |
| Atmospheric pressure | $c_P$ | 2.742 | 3.697 | 3.866 | 2.880 | hPa |
| | $\phi_{P1}$ | 1.395 | 1.288 | 1.415 | 1.497 | - |
| | $\phi_{P2}$ | −0.095 | −0.097 | −0.129 | −0.220 | - |
| | $\phi_{P3}$ | −0.303 | −0.195 | −0.290 | −0.280 | - |
| | $\sigma^2_{e_P}$ | 0.375 | 0.461 | 0.088 | 0.151 | hPa$^2$ |
| Precipitation | $f_{Hij}$ | $\begin{bmatrix} 38081 & 1028 \\ 1028 & 3073 \end{bmatrix}$ | $\begin{bmatrix} 38205 & 687 \\ 687 & 1940 \end{bmatrix}$ | $\begin{bmatrix} 38205 & 687 \\ 687 & 1940 \end{bmatrix}$ | $\begin{bmatrix} 38205 & 687 \\ 687 & 1940 \end{bmatrix}$ | − |
| | $\alpha_{\Lambda_\mathrm{p}}$ | 1.922 | 1.672 | 1.109 | 1.425 | − |
| | $\beta_{\Lambda_\mathrm{p}}$ | 0.158 | 0.188 | 0.495 | 0.280 | mm$^{-1}$ |
| Wind | $\mu_{\Theta_\mathrm{w}}$ | 2.771 | 2.839 | 3.239 | 2.561 | rad |
| | $c_\mathrm{w}$ | $\begin{bmatrix} 0.176 \\ -0.123 \end{bmatrix}$ | $\begin{bmatrix} 0.281 \\ -0.123 \end{bmatrix}$ | $\begin{bmatrix} 0.332 \\ -0.138 \end{bmatrix}$ | $\begin{bmatrix} 0.201 \\ -0.126 \end{bmatrix}$ | km h$^{-1}$, rad |
| | $\Phi_{\mathrm{w}1}$ | $\begin{bmatrix} 0.725 & -0.212 \\ 0.048 & 0.524 \end{bmatrix}$ | $\begin{bmatrix} 0.765 & -0.013 \\ 0.043 & 0.530 \end{bmatrix}$ | $\begin{bmatrix} 0.720 & 0.024 \\ 0.045 & 0.480 \end{bmatrix}$ | $\begin{bmatrix} 0.753 & -0.019 \\ 0.049 & 0.582 \end{bmatrix}$ | km h$^{-1}$, km$^{-1}$ h |
| | $\Phi_{\mathrm{w}2}$ | $\begin{bmatrix} 0.213 & -0.023 \\ -0.010 & 0.255 \end{bmatrix}$ | $\begin{bmatrix} 0.137 & -0.021 \\ -0.004 & 0.248 \end{bmatrix}$ | $\begin{bmatrix} 0.172 & -0.046 \\ 0.004 & 0.290 \end{bmatrix}$ | $\begin{bmatrix} 0.173 & -0.025 \\ -0.008 & 0.209 \end{bmatrix}$ | km h$^{-1}$, km$^{-1}$ h |
| | $\Sigma_{e_\mathrm{w}}$ | $\begin{bmatrix} 0.600 & 0.106 \\ 0.106 & 0.232 \end{bmatrix}$ | $\begin{bmatrix} 0.640 & 0.098 \\ 0.098 & 0.288 \end{bmatrix}$ | $\begin{bmatrix} 0.608 & 0.043 \\ 0.043 & 0.289 \end{bmatrix}$ | $\begin{bmatrix} 0.616 & 0.118 \\ 0.118 & 0.196 \end{bmatrix}$ | km$^2$ h$^{-2}$, km h$^{-1}$, rad$^2$ |

### Traffic density

| Parameter | Value (per road type) | Value (per season) | | | | Unit |
|---|---|---|---|---|---|---|
| | | Winter | Spring | Summer | Autumn | |
| $v_\mathrm{f}$ | Urban | | | $[43.7 \quad 51.1]$ | | |
| | Rural | | | $[53.4 \quad 78.0 \quad 87.8]$ | | km h$^{-1}$ |
| | Highway | | | $[97.3 \quad 99.8 \quad 112.1]$ | | |
| $\rho_\mathrm{c}$ | Urban | | | $[103.5 \quad 100]$ | | |
| | Rural | | | $[175.4 \quad 180 \quad 180]$ | | km$^{-1}$ |
| | Highway | | | $[230.4 \quad 180 \quad 250]$ | | |
| $\mu_\rho$ | Urban | $[3.4 \quad 0.9]$ | $[3.6 \quad 1.5]$ | $[4.1 \quad 1.0]$ | $[3.3 \quad 1.3]$ | |
| | Rural | $[1.1 \quad 1.2 \quad 1.8]$ | $[1.1 \quad 4.8 \quad 1.4]$ | $[1.2 \quad 2.9 \quad 1.7]$ | $[1.1 \quad 2.2 \quad 1.6]$ | km$^{-1}$ |
| | Highway | $[9.7 \quad 2.1 \quad 4.9]$ | $[10.6 \quad 2.7 \quad 4.2]$ | $[10.6 \quad 3.0 \quad 5.7]$ | $[9.5 \quad 2.2 \quad 4.2]$ | |
| $\rho_\mathrm{d}$ | Urban | $[3.4 \quad 0.7]$ | $[3.3 \quad 1.4]$ | $[4.2 \quad 1.0]$ | $[3.2 \quad 1.2]$ | |
| | Rural | $[0.9 \quad 2.3 \quad 1.6]$ | $[1.1 \quad 4.3 \quad 1.3]$ | $[1.1 \quad 4.4 \quad 1.6]$ | $[1.8 \quad 4.1 \quad 1.6]$ | km$^{-1}$ |
| | Highway | $[7.7 \quad 1.9 \quad 4.1]$ | $[10.2 \quad 2.7 \quad 3.6]$ | $[9.5 \quad 2.9 \quad 4.8]$ | $[7.5 \quad 2.0 \quad 3.6]$ | |
| $\varphi_{\rho_\mathrm{d}}$ | Urban | $[-1.4 \quad 1.7]$ | $[2.6 \quad -1.8]$ | $[-1.7 \quad -1.7]$ | $[-1.7 \quad -1.8]$ | |
| | Rural | $[-1.8 \quad 1.7 \quad -1.9]$ | $[-1.9 \quad -1.7 \quad -1.8]$ | $[-2.0 \quad 1.2 \quad -2.1]$ | $[-1.7 \quad 1.5 \quad -1.9]$ | rad |
| | Highway | $[-1.1 \quad -2.0 \quad -1.7]$ | $[-2.1 \quad -2.0 \quad -1.8]$ | $[-1.4 \quad -2.0 \quad -1.8]$ | $[-2.1 \quad -2.0 \quad -1.8]$ | |
| $\phi_\rho$ | Urban | $[0.9 \quad 0.9]$ | $[0.9 \quad 0.7]$ | $[0.9 \quad -0.8]$ | $[0.9 \quad 0.7]$ | |
| | Rural | $[0.6 \quad 0.9 \quad 0.8]$ | $[0.6 \quad 0.9 \quad 0.9]$ | $[0.6 \quad 1.0 \quad 0.9]$ | $[0.6 \quad 0.9 \quad 0.8]$ | − |
| | Highway | $[0.8 \quad 0.7 \quad 0.7]$ | $[0.8 \quad 0.6 \quad 0.8]$ | $[0.9 \quad 0.8 \quad 0.8]$ | $[0.9 \quad 0.7 \quad 0.9]$ | |
| $\sigma^2_{e_\rho}$ | Urban | $[1.3 \quad 0.3]$ | $[3.3 \quad 0.2]$ | $[2.1 \quad 0.1]$ | $[1.9 \quad 0.3]$ | |
| | Rural | $[0.2 \quad 1.5 \quad 0.6]$ | $[0.1 \quad 4.8 \quad 0.3]$ | $[0.1 \quad 4.2 \quad 0.3]$ | $[0.1 \quad 4.7 \quad 0.5]$ | km$^{-2}$ |
| | Highway | $[15.4 \quad 0.6 \quad 2.6]$ | $[10.7 \quad 1.6 \quad 1.4]$ | $[13.8 \quad 1.0 \quad 2.5]$ | $[14.8 \quad 2.0 \quad 1.4]$ | |

**Table 4**
Results from the categorical regression analysis conducted in Section 5.

| Regressor | $\beta$ | Impact (%) | sOC parameter |
|---|---|---|---|
| Intercept | 2045.30 | - | |
| $x_1^+$ | −420.28 | −41.1 | $\mu_\rho$ |
| $x_2^+$ | −10.52 | −1.03 | $\rho_d$ |
| $x_3^+$ | 17.01 | 1.66 | $\sigma_{e_\rho}^2$ |
| $x_4^{(2)}$ | −36.10 | −3.53 | Spring |
| $x_4^{(3)}$ | −131.53 | −12.86 | Summer |
| $x_4^{(4)}$ | −63.03 | −6.16 | Autumn |
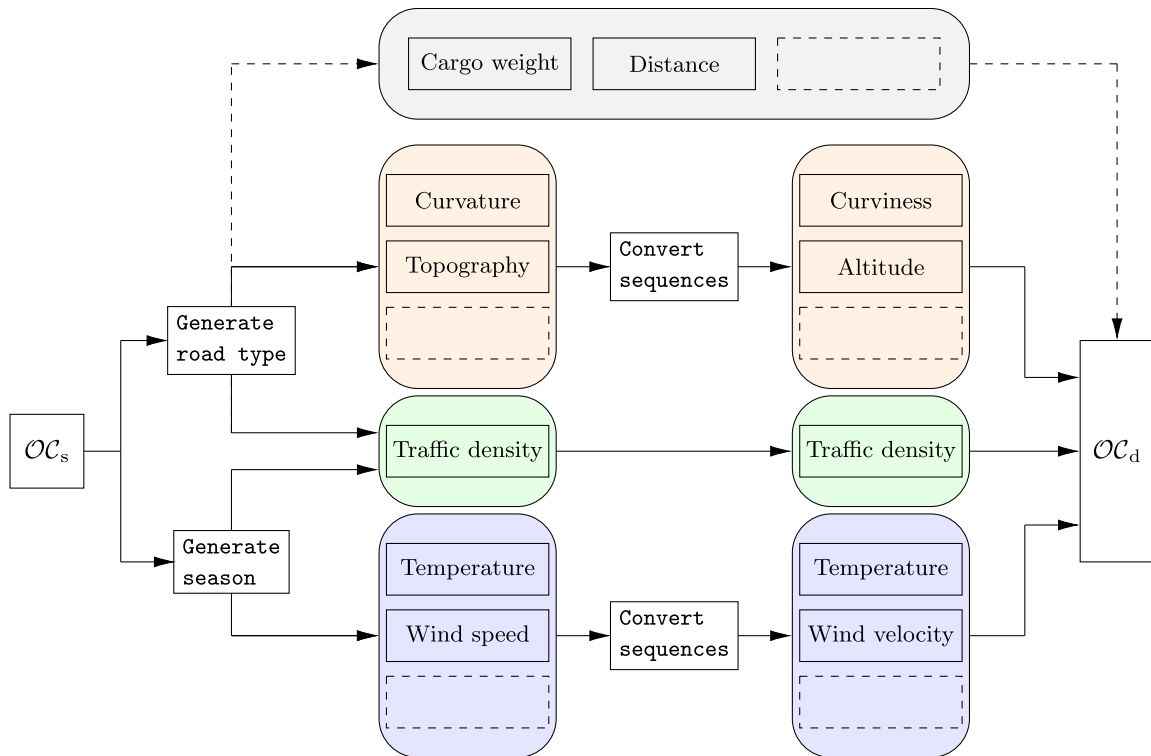


**Fig. 3.** Generation process of a deterministic operating cycle (dOC) from a stochastic one (sOC). In this paper, the mission category is assigned *a priori and is quite conventional. All the other models are generated stochastically. It should be noticed that a conversion is needed between the sOC models and the corresponding dOC parameters.*

ambient temperature. A periodic component with daily resolution may be identified, but major fluctuations are also present due to the stochastic term appearing in Eq. (8). This occasionally causes the temperature to go below zero, but these events are quite rare, even during winter. The same trend on a micro-scale may be recognised in the relative humidity time series, plotted in orange. This should not be surprising since temperature and humidity models are formally identical. Wind speed and direction (yellow and purple) are plotted before the conversion to ground level. The model consists solely of a VAR(2) process, making periodic trends harder to spot. However, it may be observed that low speed values appear to correlate to extreme directions. This might be put down to geographical reasons, but a deep analysis has not been conducted in this sense. The precipitation amount is plotted in grey. The time resolution is 15 min. Some time periods are notably more densely populated, whilst no precipitation occurs over larger intervals. This is because the model parameters (basically, the probability entries in the Markov matrix) suggest higher chances of rain for consecutive time steps. The atmospheric pressure, modelled via an AR process, is depicted in azure. Generally, it may be observed that, after an initial increase to 1040 hPa, the pressure remains constant for 3–4 days and then decreases again. This might be an isolated phenomenon, and has no particular significance. Finally, the traffic density, in green, is generated over a rural road (speed limit 70 $\mathrm{km\,h^{-1}}$) and clearly exhibits a periodic trend, as predicted by the model in SubSection 3.3. Lower densities are typical of nocturnal hours, with the peak reached sometime during the day. Analogous considerations are also valid for other seasons, but with different intensities.

    Useful, usable and easy-to-interpret data is thus generated and then formally encoded into the dOC structure, as per the conversion
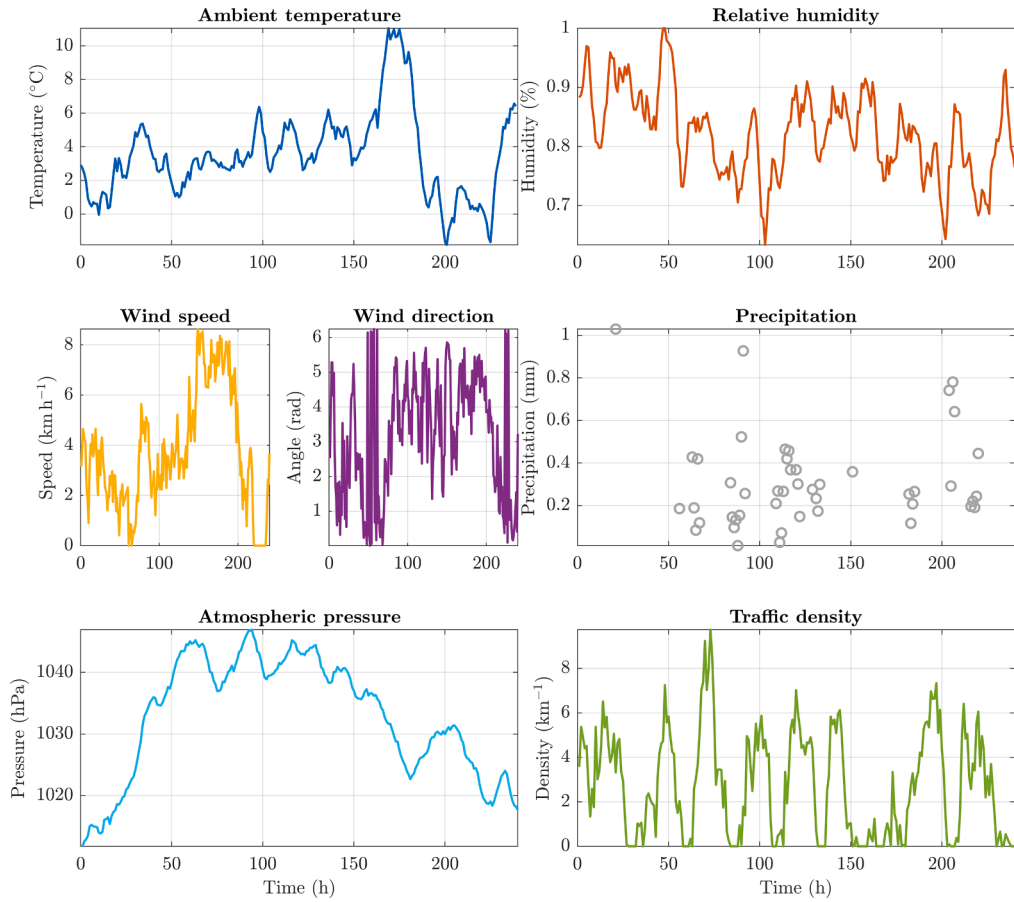
**Fig. 4.** Weather and traffic (density) categories of the stochastically generated dOC in Section 4. Time horizon: 10 days.
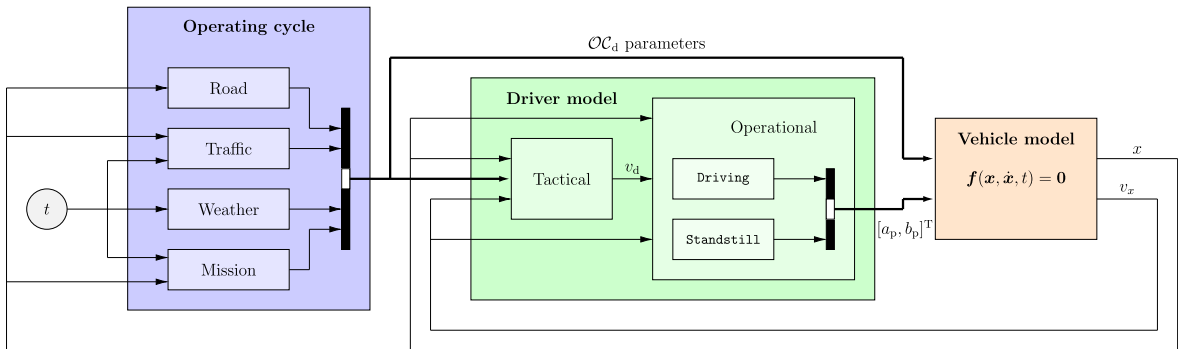


**Fig. 5.** Simulation of a dOC together with the driver and vehicle models in the VehProp environment.

mentioned earlier.

### 4.3. Simulation

To be used practically in vehicle design applications, the dOC description needs to be integrated with detailed models for both driver and vehicle, and then simulated in a virtual environment. The open-access platform VehProp, originally developed by Jacobson
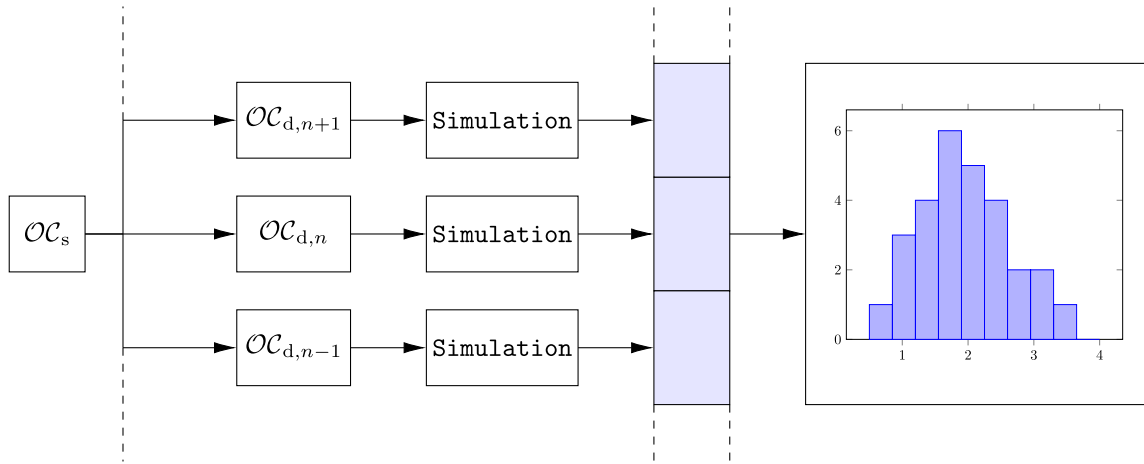
**Fig. 6.** A stochastic operating cycle (sOC) may be used to synthesise different deterministic realisations (dOCs) which share the same statistical properties. The distribution in $CO_2$ emissions produced by a specific set of sOC parameters may be evaluated by simulating each dOC and clustering the output data.

et al. (yyyy) and implemented in MATLAB/Simulink®, may serve this purpose. This was conceived as simulation tool for virtual development, testing and validation of both physical components and algorithms. Simulations in VehProp are generally much faster than real-time[12], and allow for rapid assessment of performance.

Fig. 5 illustrates the closed-loop system comprising the OC, driver and vehicle blocks. The dOC parameters generated using the procedure outlined in Section 4.2 are encoded in MATLAB® tables. These may be regarded as two or three-dimensional matrices, depending on the OC category. Thus, the indices of each physical quantity are associated with discrete positions $x_i$ and/or times $t_i$. Values in between are interpolated using the models listed in Table 1.

The dOC parameters calculated at each time step and position along the vehicle's trajectory are used as input to the driver model. This is split into a tactical and an operational component. The first one interprets the dOC parameters and translates them into a desired speed signal $v_d$, mostly based on static physical models. The overall logic behind this process is explained in greater detail in Appendix A. The operational part of the driver – modelled in this paper as a PID controller – estimates the desired output in terms of acceleration and brake pedal position $a_p, b_p \in [0, 1]$ starting from the error between the desired speed and the actual one. More detailed illustrations of both the driver and vehicle modules are given in Figs. 9 and 10 in Appendix A.

The pedal position, plus the dynamically calculated dOC parameters, constitute the input to the longitudinal vehicle model, which is essentially a system of differential–algebraic equations (DAE) in the form $f(x, \dot{x}, t) = 0$. More specifically, the vehicle model used in this paper assumes zero tyre slips, and therefore the longitudinal dynamics is assimilated to that of a point-mass particle, as described in Appendix A (more complex formulations can be found in e.g. Pettersson et al. (2016), Romano et al. (2021)). Furthermore, the contribution from auxiliary equipment is not considered at this stage[13]. Two different sets of equations are used to cope with standstill. The output from these sets of equations is the longitudinal acceleration. By straightforward integration, the speed $v_x$ and position $x$ are deduced dynamically, and returned to the OC and driver blocks. Indeed, the current position $x$ constitutes the primary input to all the dOC parameters in the categories $\mathscr{R}_d, \mathscr{M}_d$ and $\mathscr{T}_d$.

## 5. Sensitivity analysis on energy efficiency

A concrete application example is now presented to illustrate the potential of the novel sOC format when used in combination with VehProp. This means investigating the impact of weather and traffic conditions on the $CO_2$ emissions of a reference truck, given a constant set of road parameters. In this context, it is important to remark that each dOC originating from the same sOC shares the same statistical properties, and is hence statistically equivalent. This makes the OC framework idoneous to studying, say, spread in fuel consumption and $CO_2$ emissions. A graphical illustration of the process is schematised in Fig. 6: a unique set of stochastic parameters is used to generate several dOCs, seen as independent realisations. These are simulated in VehProp, yielding different results in terms of numerical output. This results in a distribution, for which is possible to estimate the relevant statistical properties.

The underlying idea behind the following example is to keep all the road properties listed in Table 1 constant and vary the weather and traffic parameters. Since the weather properties are grouped together in the season model, they will only be distinguished based on

---

[12] For the examples proposed in Section 5, the total simulation time per generated dOC ranged between 2 and 4 min using ODE45 on a personal laptop.

[13] It is noteworthy that these are components of the vehicle and not directly part of the format. In any case, the vehicle model may be improved in future studies.

**Table 5**
sOC traffic parameter for the high setting.

| Parameter | Value (per road type) | Traffic parameters | | | | Unit |
|---|---|---|---|---|---|---|
| | | Value (per season) | | | | |
| | | Winter | Spring | Summer | Autumn | |
| $\mu_\rho$ | Urban | $[55.2 \quad 50.9]$ | $[55.4 \quad 51.5]$ | $[55.9 \quad 51.0]$ | $[55.1 \quad 51.3]$ | |
| | Rural | $[88.8 \quad 91.2 \quad 91.8]$ | $[88.8 \quad 94.8 \quad 91.4]$ | $[88.9 \quad 92.9 \quad 91.7]$ | $[88.8 \quad 92.2 \quad 91.6]$ | $km^{-1}$ |
| | Highway | $[124.9 \quad 92.1 \quad 124.9]$ | $[125.8 \quad 92.7 \quad 124.2]$ | $[125.8 \quad 93.0 \quad 125.7]$ | $[124.7 \quad 92.2 \quad 124.2]$ | |
| $\rho_d$ | Urban | $[13.6 \quad 2.8]$ | $[13.2 \quad 5.6]$ | $[16.8 \quad 4.0]$ | $[12.8 \quad 4.8]$ | |
| | Rural | $[3.6 \quad 9.2 \quad 6.4]$ | $[4.4 \quad 17.2 \quad 5.2]$ | $[4.4 \quad 17.6 \quad 6.4]$ | $[7.2 \quad 16.4 \quad 6.6]$ | $km^{-1}$ |
| | Highway | $[30.8 \quad 7.6 \quad 16.4]$ | $[40.8 \quad 10.8 \quad 14.4]$ | $[38.0 \quad 11.6 \quad 19.2]$ | $[30.0 \quad 8.0 \quad 14.4]$ | |
| $\sigma_{e_\rho}^2$ | Urban | $[5.2 \quad 1.2]$ | $[13.2 \quad 0.8]$ | $[8.4 \quad 0.4]$ | $[7.6 \quad 1.2]$ | |
| | Rural | $[0.8 \quad 6.0 \quad 2.4]$ | $[0.4 \quad 17.2 \quad 1.2]$ | $[0.1 \quad 4.2 \quad 0.3]$ | $[0.1 \quad 4.7 \quad 0.5]$ | $km^{-2}$ |
| | Highway | $[61.6 \quad 2.4 \quad 10.4]$ | $[42.8 \quad 6.4 \quad 5.6]$ | $[55.2 \quad 4.0 \quad 10.0]$ | $[59.2 \quad 8.0 \quad 5.6]$ | |
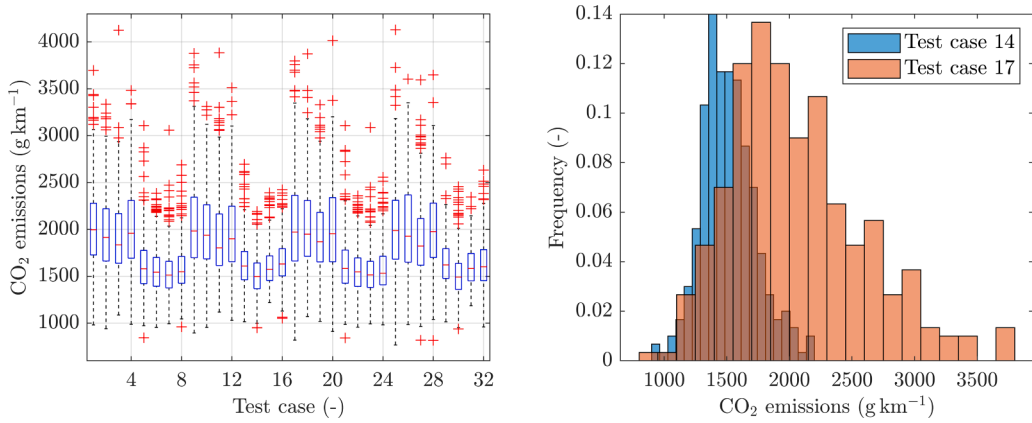


**Fig. 7.** Results from the sensitivity study conducted in Section 5. The boxplots (left) show a correlation between the external settings and $CO_2$ emissions, which seem to decrease with higher traffic densities and during milder seasons. The histograms on the right compare the two TCs with the overall lowest (14 in blue) and highest (17 in orange) mean $CO_2$ emissions. TC 14 refers to the setting in which all the traffic parameters are high, except for the variance $\sigma_\rho^2$. Conversely, in TC 17 all the traffic parameters, except $\sigma_\rho^2$, are low. The two TCs also differ for seasonality: spring for TC 14 and winter for TC 17.

their corresponding primary sOC parameter, i.e. seasonality. This allows a considerable reduction in the number of variables involved.

Instead, this paper constrains itself to commenting on the implications of adding the novel stochastic descriptions for weather and traffic to the OC.

To understand the implications of varying the weather parameters, one may start by looking at Eqs. (1) and (2c). The wind speed and direction, showing directly in Eq. (2c), presumably have the highest impact on the term $F_{air}$. On the other hand, the ambient temperature and pressure will both modify the air density $\rho_{air}$, but with only minor anticipated effect. The other weather parameters, albeit dynamically included in the format, will not affect the emissions, since there is no model to account for their effect. For example, the influence of humidity over the engine efficiency does not currently feature in the vehicle model. Similar considerations hold true for auxiliary components and power demands, such as heating and AC. These are not considered in the present study. Analogously, at this stage, the tactical part of the driver does not incorporate any model to replicate reductions in speed due to precipitation. Thus, in the following analysis, the only parameters of interest are wind speed and direction, ambient temperature and atmospheric pressure.

For the traffic, the situation is more complicated and the interpretation is less straightforward. For this, the authors have decided to vary the three main parameters which are anticipated to have the most significant influence on the vehicle's speed and energy efficiency: average traffic density $\rho_t$, amplitude over the day $\rho_d$ and variance of the innovation $\sigma_{e_\rho}^2$. The combined effect of these quantities will determine the desired speed input to the tactical part of the driver model (see Appendix A) through Eq. (26), which will react accordingly. In the test design, each traffic parameter is allowed to assume a low value (corresponding to the nominal one listed in Table 3 and a high one. Specifically, for each combination of road type and legal speed, the high setting for the parameter $\mu_\rho$ is obtained by adding the term $\rho_c/2$, which, as mentioned previously, corresponds to the value of the density making the transition between free-flow and congested traffic regimes. The parameters $\rho_d$ and $\sigma_{e_\rho}^2$ are instead multiplied by 4 in the high setting, as also reported in Table 5 (see Appendix B). The total number of possible combinations is thus $4 \cdot 2^3 = 32$. For each test case (TC), 300 missions each with 27

**Table 6**
Parameters setting for each TC in Section 5.

| TC | $x_1$ | $x_2$ | $x_3$ | $x_1$ |
|----|-------|-------|-------|-------|
| 1 | −1 | −1 | −1 | 1 |
| 2 | −1 | −1 | −1 | 2 |
| 3 | −1 | −1 | −1 | 3 |
| 4 | −1 | −1 | −1 | 4 |
| 5 | 1 | −1 | −1 | 1 |
| 6 | 1 | −1 | −1 | 2 |
| 7 | 1 | −1 | −1 | 3 |
| 8 | 1 | −1 | −1 | 4 |
| 9 | −1 | 1 | −1 | 1 |
| 10 | −1 | 1 | −1 | 2 |
| 11 | −1 | 1 | −1 | 3 |
| 12 | −1 | 1 | −1 | 4 |
| 13 | 1 | 1 | −1 | 1 |
| 14 | 1 | 1 | −1 | 2 |
| 15 | 1 | 1 | −1 | 3 |
| 16 | 1 | 1 | −1 | 4 |
| 17 | −1 | −1 | 1 | 1 |
| 18 | −1 | −1 | 1 | 2 |
| 19 | −1 | −1 | 1 | 3 |
| 20 | −1 | −1 | 1 | 4 |
| 21 | 1 | −1 | 1 | 1 |
| 22 | 1 | −1 | 1 | 2 |
| 23 | 1 | −1 | 1 | 3 |
| 24 | 1 | −1 | 1 | 4 |
| 25 | −1 | 1 | 1 | 1 |
| 26 | −1 | 1 | 1 | 2 |
| 27 | −1 | 1 | 1 | 3 |
| 28 | −1 | 1 | 1 | 4 |
| 29 | 1 | 1 | 1 | 1 |
| 30 | 1 | 1 | 1 | 2 |
| 31 | 1 | 1 | 1 | 3 |
| 32 | 1 | 1 | 1 | 4 |

tonne payload are generated over a distance of 125 km. Each mission is, in turn, mirrored to ensure a balance in the potential (gravitational) energy. The vehicle specification is based on a heavy-duty truck of the kind commonly used for log-haul missions; specifically, a Volvo FH13 equipped with a diesel engine, an actuated, stepped gearbox with 12 forward gears and a kerb weight of 7540 kg. Additional information about the vehicle's configuration can be found in the Volvo datasheets[14].

CO$_2$ emissions are calculated in VehProp starting from the total mass of fuel obtained from Eq. (34). Simulation results are shown in Fig. 7. In the boxplot (left-hand diagram), the median emissions are depicted in red, with the blue boxes covering results between the 25 and 75th percentiles and the dotted lines encompassing the overall range. It can be clearly seen that changes in the external settings are reflected in the CO$_2$ emissions. Two main conclusions can be drawn by looking at Fig. 7. The first relates to variations due to traffic conditions, the second to changes in seasonality. Indeed, based on their periodic trends, the boxplots can be separated into subgroups of four TCs for which the parameter $\mu_\rho$ is in the low or high setting (low for odd subgroups, high for even). Each TC in a subgroup is then characterised by the same setting for the traffic parameters but with different seasonality. Hence, it can be inferred that higher $\mu_\rho$ values cause the emissions to decrease. This can be explained by observing that the traffic model used in this paper only consists of a macroscopic representation, and does not capture stop-and-go patterns occurring on the micro scale. Therefore, the effect of higher traffic densities is to reduce the vehicle's speed towards ranges within which the engine is more efficient.

Seasonality also seems to play some systematic role in CO$_2$ variations, with spring and summer often characterised by lower values than winter and autumn. Apart from the contributions relating to wind parameters, one explanation might be that a secondary effect of milder temperatures is a decrease in the air density according to Eq. (5), and thus also the drag force in Eq. (1).

Two distributions, referring to the TC with lowest (14) and highest (17) mean emissions, are shown in the right-hand diagram of Fig. 7. In TC 14 the setting for the mean traffic density $\mu_\rho$ is on the high value, as opposed to TC 17. They also differ for other traffic parameters and seasonality settings (spring for TC 14 and winter for 17). From Table 6, it can be observed that the values for $\mu_\rho$ and $\rho_d$

---

**Table 7**
Additional data for the sensitivity analysis of Section 5.

| TC | CO$_2$ emissions (g km$^{-1}$) | | | | | | |
|---|---|---|---|---|---|---|---|
| | Mean | SD | 25th percentile | Median | 75th percentile | Min | Max |
| 1 | 2043 | 474 | 1728 | 1997 | 2279 | 981 | 3699 |
| 2 | 1978 | 423 | 1663 | 1915 | 2221 | 940 | 3337 |
| 3 | 1920 | 407 | 1639 | 1834 | 2169 | 1086 | 4126 |
| 4 | 2004 | 439 | 1693 | 1960 | 2308 | 988 | 3483 |
| 5 | 1626 | 302 | 1422 | 1579 | 1776 | 844 | 3108 |
| 6 | 1572 | 261 | 1393 | 1544 | 1701 | 955 | 2386 |
| 7 | 1546 | 254 | 1376 | 1513 | 1659 | 994 | 3058 |
| 8 | 1579 | 272 | 1425 | 1548 | 1712 | 960 | 2689 |
| 9 | 2048 | 497 | 1698 | 1983 | 2344 | 895 | 3878 |
| 10 | 2006 | 453 | 1686 | 1939 | 2263 | 955 | 3311 |
| 11 | 1914 | 452 | 1615 | 1803 | 2165 | 1185 | 3885 |
| 12 | 1952 | 460 | 1656 | 1901 | 2248 | 1030 | 3512 |
| 13 | 1643 | 280 | 1463 | 1609 | 1765 | 1015 | 2696 |
| 14 | 1514 | 217 | 1368 | 1498 | 1642 | 948 | 2192 |
| 15 | 1615 | 228 | 1455 | 1575 | 1718 | 1218 | 2391 |
| 16 | 1663 | 246 | 1504 | 1632 | 1794 | 1051 | 2424 |
| 17 | 2059 | 535 | 1663 | 1972 | 2363 | 818 | 3797 |
| 18 | 2016 | 459 | 1713 | 1949 | 2308 | 1070 | 3872 |
| 19 | 1949 | 424 | 1654 | 1867 | 2182 | 1019 | 3330 |
| 20 | 2018 | 461 | 1655 | 1955 | 2339 | 911 | 4013 |
| 21 | 1629 | 302 | 1426 | 1583 | 1779 | 843 | 3106 |
| 22 | 1570 | 261 | 1391 | 1547 | 1696 | 957 | 2358 |
| 23 | 1548 | 252 | 1381 | 1515 | 1659 | 992 | 3086 |
| 24 | 1576 | 273 | 1408 | 1533 | 1714 | 981 | 2557 |
| 25 | 2034 | 495 | 1682 | 1987 | 2311 | 767 | 4129 |
| 26 | 2018 | 502 | 1650 | 1927 | 2367 | 985 | 3603 |
| 27 | 1906 | 442 | 1618 | 1823 | 2116 | 819 | 3594 |
| 28 | 1988 | 447 | 1700 | 1976 | 2281 | 816 | 3649 |
| 29 | 1647 | 261 | 1477 | 1621 | 1794 | 1014 | 2763 |
| 30 | 1522 | 253 | 1361 | 1492 | 1637 | 938 | 2458 |
| 31 | 1604 | 217 | 1451 | 1583 | 1743 | 1186 | 2346 |
| 32 | 1638 | 278 | 1453 | 1601 | 1784 | 959 | 2634 |

**Table 8**
Results from the categorical regression analysis conducted in Section 5.

| Variable | $\beta$ | tStat | pValue |
|---|---|---|---|
| Intercept | 2045.30 | 122.5 | 0 |
| $x_1^+$ | −420.28 | −22.39 | $\ll 10^{-3}$ |
| $x_2^+$ | −10.52 | −0.56 | 0.57512 |
| $x_3^+$ | 17.01 | 0.91 | 0.36481 |
| $x_4^{(2)}$ | −36.10 | −1.67 | 0.095928 |
| $x_4^{(3)}$ | −131.53 | −6.07 | $\ll 10^{-3}$ |
| $x_4^{(4)}$ | −63.03 | −2.91 | 0.0036464 |
| $x_1^+ x_2^+$ | 40.18 | 2.62 | 0.008764 |
| $x_1^+ x_3^+$ | −18.33 | −1.20 | 0.2317 |
| $x_1^+ x_4^{(2)}$ | −50.35 | −2.32 | 0.02021 |
| $x_1^+ x_4^{(3)}$ | 65.21 | 3.00 | 0.0026347 |
| $x_1^+ x_4^{(4)}$ | 32.85 | 1.52 | 0.1297 |
| $x_2^+ x_3^+$ | −11.64 | −0.76 | 0.44741 |
| $x_2^+ x_4^{(2)}$ | −22.46 | −1.04 | 0.30002 |
| $x_2^+ x_4^{(3)}$ | 15.37 | 0.70 | 0.47833 |
| $x_2^+ x_4^{(4)}$ | 11.9 | 0.54 | 0.58305 |
| $x_3^+ x_4^{(2)}$ | 12.21 | 0.56 | 0.57315 |
| $x_3^+ x_4^{(3)}$ | 1.05 | 0.05 | 0.96154 |
| $x_3^+ x_4^{(4)}$ | 3.43 | 0.16 | 0.87432 |

(a) Main effects.



(b) First-order interaction.
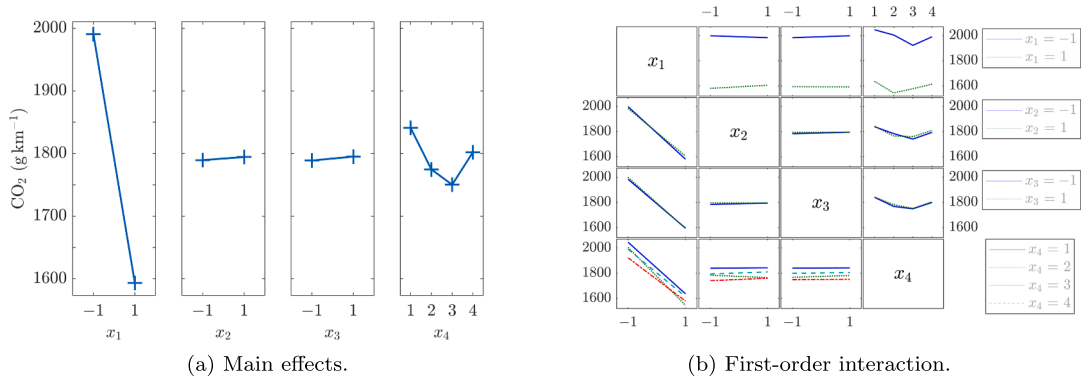
**Fig. 8.** Graphical illustration of the regression analysis conducted in Section 5. The first subplot (left) represents the main effect, the second one (right) the first-order interaction between the categorical variables. In particular, $x_1, x_2$ and $x_3$ refer to the physical quantities $\mu_\rho, \rho_d$ and $\sigma^2_{e_\rho}$; the fourth variable $x_4$, ranging from 1 to 4, refers to the season index (1 for winter, 2 for spring, 3 for summer and 4 for autumn).

contribute to the relatively high traffic density, but with smaller fluctuations. This results in the lowest possible mean emission (1514 $g\,km^{-1}$), with a contained standard deviation (SD) of 217 $g\,km^{-1}$. On the other hand, in TC 17, all the traffic parameters are set low, with the exception of $\sigma^2_{e_\rho}$. The corresponding mean and SD are the highest possible: 1514 and 535 $g\,km^{-1}$. This result aligns with the previous observations: the truck tends to drive faster and the $CO_2$ increases accordingly. Finally, additional results for all the TCs are summarised in Table 7.

The contribution from each parameter, or group of parameters, to the total $CO_2$ emissions is quantified by conducting a regression analysis. The traffic parameters $\mu_\rho, \rho_d$ and $\sigma^2_{e_\rho}$ are treated as categorical variables $x_i, i = 1, 2, 3$, assuming value $-1$ for the low setting and 1 for the high one. Another variable $x_4$, assuming integer values from 1 to 4, refers to the season index (1 for winter, 2 for spring, 3 for summer and 4 for autumn) and takes into account the influence of the weather parameters. The categorical analysis is conducted assuming as reference scenario the one in which all the traffic parameters are on the low setting and the season is winter. This basically corresponds to the first TC1.

Based on the above premises, and assuming a first order interaction, the response $y$ given in terms of $CO_2$ emissions is then expressed as:

$$y = \beta_0 + \sum_{i=1}^{3} \beta_i x_i^+ + \sum_{i=1}^{3} \beta_{i+3} x_4^{(i+1)} + \sum_{i=1}^{2} \sum_{j=i+1}^{3} \beta_{ij} x_i^+ x_j^+ + \sum_{i=1}^{3} \sum_{j=2}^{4} \beta_{i4} x_i^+ x_4^{(j)} + \varepsilon,$$ (27)

where $\beta$ are the regression coefficients and $\varepsilon$ is the residual. The meaning of the variables $x_i^{(+)}$ appearing in the above Eq. (27) is promptly explained: they assume value 0 if the corresponding variable $x_i$ is on the low setting, and 1 if the associated $x_i$ is on the high setting. Something analogous happens for the variable $x_4^{(2)}, x_4^{(3)}$ and $x_4^{(4)}$ encoding the information about weather: they assume value 1 if the season in the TC is spring, summer or autumn; otherwise 0. Therefore, if all the variables showing in (27) assume value of 0, the scenario corresponds to that being referenced and the computed variation is also 0. The complete results from the categorical regression analysis are listed in Table 8. In Table 4, the only the main effect is reported, where the impact of each regressor is also interpreted as the percentage $2\beta_i/\beta_0$. The latter ratio is an indicator of the variation in $CO_2$ emissions between the low and high settings for each parameter, given that all the others are as in the reference scenario. It can be concluded from Table 4 that the most influential parameter is the mean density $\mu_\rho$. This corroborates some previous considerations. The other traffic parameters do not seem to play a crucial role in the spread of emissions, whilst the effect of seasonality appears to be more relevant. Indeed, it may be observed that, according to the data reported in Table 4, winter is the season characterised by the highest emissions. Any change introduced into the seasonal settings is responsible for a negative variation, with the summer being in first position with a percentage reduction of 12.86%, followed by autumn and spring (6.16 and 3.53, respectively).

Coming back to the original variables $x_i$, a graphical interpretation of their contribution is shown in Fig. 8. The main effect for each variable is shown on the left. It can be observed that the first one, encoding information on the mean density, produces the greatest variation between the low and high settings, consistent with what discussed before. This result seems to contradict previous findings in literature. Indeed, based on the measured data of Song et al. (2016), higher traffic density values are expected to cause the emission to increase. There are two main arguments justifying this discrepancy. The first is that, as already mentioned, the fundamental relationship of Eq. (26) was parametrised using data available only for the upper part of the diagram. Therefore, there is no guarantee that the low-regime speeds have been reproduced satisfactorily in the present study. Furthermore, the OC representation is currently unable to replicate stop-and-go patterns which occur at low speed, which are the main cause of increased emissions. On the other hand, the (almost) constant low speeds postulated by Eq. (26) produce the opposite effect.

The response to the other traffic parameters $\rho_d$ and $\sigma^2_{e_\rho}$ exhibits a similar linear behaviour, albeit much less evident. The relationship is, instead, convex with respect to the seasonality, with the minimum obtained somewhere around summer. As outlined before, a

possible explanation is that the temperature also affects the air resistance, but there are many other interacting factors, e.g. seasonal traffic and wind speed and direction, whose contribution is harder to interpret.

The secondary effect due to the interaction between the variables is illustrated in the right-hand subplot of Fig. 8. The most interesting aspect relates to the interaction between $x_1$, representing the mean density $\mu_\rho$ and the seasonality. It may be observed that the response is still convex, but the minimum moves to the left when $x_1$ is on the high setting. To understand this, the values of $\mu_\rho$ (listed in Table 3) may be examined. Spring and summer are characterised by similar mean densities for given combinations of road type and legal speeds. Therefore, a simple explanation is that the minimum is actually attained for some month between these two seasons. However, the regression analysis is unable to capture the variation at such scale. Accordingly, two different minima are predicted for discrete values of $x_4$. The same phenomenon takes place for the amplitude $\rho_d$, whilst the minimum for the variance $\sigma_{e_\rho}^2$ is always around spring.

## 6. Discussion

Firstly, this section discusses the main limitations of the OC format in the context of vehicle design applications and looks at opportunities for further improvement. Secondly, it examines a prospective application for the OC representation at county and national levels, for legislative purposes.

### 6.1. Limitations and future work

In the present paper, the enhanced sOC description has been used to investigate variations in pollutant emissions due to different driving conditions. The current version of the OC format is much more complete than the original formulation, but there are still some identifiable areas for improvement. Some limitations clearly emerge when considering the results of the sensitivity study conducted in Section 5. Indeed, it has been shown that $CO_2$ emissions decrease during milder seasons (spring and summer), and as traffic density increases. With reference to the first phenomenon, a convincing explanation can be found by considering that higher temperatures imply lower air density values, thus reducing air resistance. Traffic conditions are also expected to have a major influence on $CO_2$ emissions, since they determine the driver's speed choice. However, the study's findings are in contrast with empirical observations Song et al. (2016). This should be mainly ascribed to the traffic model included in the sOC representation, which is based on a macroscopic approach and unable to capture micro-scale stop-and-go patterns. Furthermore, the fundamental relationship used in the paper has only been partially validated against real data. As already pointed out, this is a limitation of the present study, and deserves further investigation. The possibility of using different fundamental diagrams depending on the road type (e.g. urban, rural or highway) definitely warrants future consideration.

Moreover, whilst the current sOC framework collects models for the road, weather and traffic categories, there is still no stochastic description of the transport mission itself. This aspect constitutes an interesting opportunity for further research. Statistical models for the mission category might be constructed using a similar approach to those proposed, for example, in Kivekas et al. (2018), Kivekas et al. (2017), which considered variations in stops and passenger load.

Another area of improvement relates to the need for deterministic models accounting for the influence of sOC parameters on the physical quantities affecting a vehicle's behaviour. For example, the rolling resistance coefficient depends on both weather and road conditions, but no explicit model has been presented in this study. Similar considerations may be extended to auxiliary components not considered in this paper.

The application of the enhanced sOC format is not limited to energy efficiency studies. The possibility of using it for optimisation purposes must be fully explored and is certainly an interesting direction to explore. The idea is to replace the customary approach considering a given speed profile with one which incorporates current information (and possibly also prediction) about the surroundings. This could substantially improve the robustness and efficacy of algorithms and functions. In the context of product development, it would also be beneficial to construct maps and databases of different sOC sets. Thus, if the boundary conditions (here intended as the operating environment) are known (at least in a statistical sense) the design of a vehicle may be tailored to satisfy the specific requirements for those settings. The paper has outlined the concept in general terms but it does warrant deeper investigation. Another interesting aspect to address relates to the need for mission classification. Indeed, labels and limits must also be imposed, depending on the characteristics of the mission concerned. Even within the same geographical area and seasonal setting, these may differ. The reverse aspect is also worth exploring. A classification process of the environmental properties may be conducted by using data collected from instrumented vehicles. This would also help municipalities and other organisations to plan interventions with, and maintenance of, the road infrastructure.

### 6.2. Discussion on policy implications

In strict connection with the above, the OC description might also be used for legislative purposes at county and national levels. As already mentioned in the introduction, many tools currently in usage make use of the concept of driving cycle to accurately predict $CO_2$ emissions. These include the VECTO, CMEM and VSP models. In this context, the OC representation certainly represents an interesting alternative, albeit not necessarily a viable one. Indeed, parametrising an sOC is difficult, as estimating road, traffic and weather parameters requires a large dataset. These difficulties may be overcome if different partners collaborate in a joint effort. For example, data may be supplied to municipalities and environmental agencies by specialist organisations, like Trafikverket and SMHI in Sweden.

The accessibility of vast amounts of data is a prerequisite in making the OC applicable for legislation purposes, and posed a major limitation to the present study.

## 7. Conclusions

This paper has extended the stochastic operating cycle (sOC) description to include models for both the weather and traffic categories. The current form of sOC introduced by the authors represents a road transport mission with its surroundings as a collection of stochastic parameters arranged hierarchically. These models condense the statistical characteristics of the operation and its settings, and have been developed to be mutually independent. Nonetheless, the interaction between the involved physical quantities is accounted for by splitting the set of available models into primary and secondary ones. Road type and season belong to the first subset. The introduction of the seasonal setting is new in respect to the original sOC, also allowing time variations to be captured. Hence, the complete framework is defined as a structured composition of secondary road, traffic, weather and mission parameters, which inherit their properties from the primary models. The resulting composite structure allows for ease of implementation and preserves modularity. Therefore, the format itself may be further extended, or even reduced, without any intervention in the existing models.

The new sOC has been parametrised using free data collected from weather and traffic stations. The fitting procedure has been conceived to be as simple as possible, requiring only standard packages implemented in MATLAB®. Details have been presented on how to generate multiple deterministic descriptions of an operating cycle, called dOC, starting from a suitable set of sOC parameters. Generating synthetic dOCs allows virtual prototypes to be tested under more general conditions than those in a conventional driving cycle. Furthermore, when integrated with a dynamic simulation model, like VehProp, the sOC format can be used to conduct energy efficiency studies as well as developing ad hoc functions and algorithms which factor in environmental influences. To illustrate the potential of the enhanced sOC, a regression analysis was conducted to quantify variations in CO2 emissions due to modifications to the operating environment. To limit the scope of the paper, only the influence of the seasonal and traffic settings were considered. Results from the analysis highlighted the fact that both seasonality and traffic conditions introduce major variations into $CO_2$ emissions.

## Appendix A. Driver and vehicle models

The detailed equations for the driver and vehicle models used in this paper are given here.

### A.1. Driver model

The driver model is split into a tactical and an operational part. The former interprets the OC parameters based on simplified physical models and translates them into a desired speed input for the operational driver. At each time step and position, the final desired speed $v_d$ is chosen as:

$$v_d = \min\left(v_{sign}, v'_{sign}, v_\kappa, v'_\kappa, v_b, v'_b, v_{stop}, v'_{stop}, v_t, v'_t\right). \tag{28}$$

where the generic $v_p$ is function of the OC parameters, i.e. $v_p = f_p(\mathscr{OC}_d)$. More specifically, the speeds $v_{sign}, v_\kappa, v_b$ and $v_{stop}$ correlate with the legal speed limit, road curvature $\kappa$, speed bumps and stops, respectively. The corresponding functions $f_p(\cdot)$ are given in Pettersson et al. (2019). The traffic speed $v_t \equiv v_e$ introduced in this paper is determined by using Eq. (26). Furthermore, for each speed $v_p$, a corresponding *dynamic* value is calculated as

$$v'_p = \sqrt{v_{p,i+1} - 2a_x^{max}(x_{i+1} - x)}, \tag{29}$$

where $x$ is the current position, $x_{i+1}$ the next (discrete) position value at which the speed $v_p$ changes value, and $a_x^{max}$ is the acceleration threshold. Once the desired speed has been set, the operational part of the driver computes the difference between desired and the actual speed to produce the pedal outputs $a_p, b_p \in [0, 1]$. In this paper, the operational part of the driver is modelled using a PID controller. Specifically, the expressions for $a_p$ and $b_p$ read as follows:

$$a_p = \frac{1}{2}f_{PID}\left(v_d - v_x\right)[1 + sgn(f_{PID}(v_d - v_x))], \tag{30a}$$

$$b_p = -\frac{1}{2}f_{PID}\left(v_d - v_x\right)[1 - sgn(f_{PID}(v_d - v_x))], \tag{30b}$$

where $f_{PID}(\cdot)$ is the function describing the PID control law.

A graphical illustration of the driver module, together with the input and output quantities, is given in Fig. 9.

*A.2. Vehicle model*

The vehicle model used in this paper neglects the tyre slip, from which condition we deduce $F_x = (T_d - T_b \text{sgn}(v_x))/R_w$ in Eq. (1), where $T_d$ and $T_b$ are the total driving torque reported at the wheels and the braking torque, respectively. Therefore, the governing equations for the longitudinal vehicle dynamics can be derived starting from Eq. (1) as follows:

$$m^* \dot{v}_x = \frac{T_d - T_b \text{sgn}(v_x)}{R_w} - F_{\text{grade}} - F_{\text{roll}} - F_{\text{air}}, \qquad v_x \neg = 0, \tag{31a}$$

$$F_b = F_{\text{grade}} + F_{\text{roll}} + F_{\text{air}} - \frac{T_d}{R_w}, \qquad |F_b| \leqslant \frac{T_b}{R_w}, \tag{31b}$$

with the resistive forces reading as in Eq. (2). Eqs. (31a) and (31b) are valid under normal driving conditions and at standstill. The torques $T_d$ and $T_b$ in Eqs. (31) are calculated starting from the engine torque $T_e$ and the output from the operational part of the driver as

$$T_d = \eta_t i_g i_{\text{FD}} \left( T_e - \frac{P_{\text{PTO}}}{\omega_e} \right), \tag{32a}$$

$$T_b = T_b^{\max} b_p, \tag{32b}$$

where $i_g$ and $i_{\text{FD}}$ are the gear ratio and final drive gear, and $\eta_t$ is the overall efficiency of the transmission. In turn, the engine torque $T_e$ is
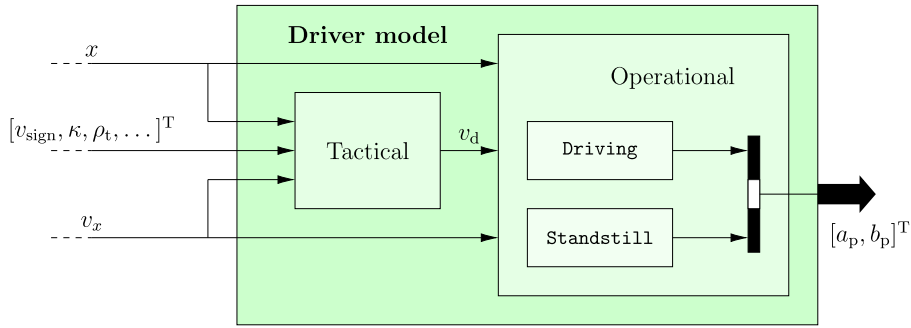


**Fig. 9.** Schematic representation of the driver model. The inputs to the module are the vehicle's longitudinal speed and position $[v_x, x]^T$ and the $\mathscr{CC}_d$ parameters which determine the speeds in Eq. (28). The outputs are the acceleration and brake pedal positions $[a_p, b_p]^T$.

modelled using steady-state maps as a function of the engine speed $\omega_e$ and fuel injection $q$:

$$T_{\text{req}} = T_e^{\max} a_p, \tag{33a}$$

$$q = f_q(\omega_e, T_{\text{req}}), \tag{33b}$$

$$T_e = f_T(\omega_e, q), \tag{33c}$$

where the mappings $f_T(\cdot, \cdot)$ and $f_q(\cdot, \cdot)$ are given in the form of look-up tables.

From Eqs. (33), the total mass of fuel may be calculated as

$$m_f = \int_{t_0}^{t_f} \gamma \omega_e q \, dt, \tag{34}$$

in which $t_0$ and $t_f$ are the initial and final times, and $\gamma$ is a proportionality constant. The corresponding mass of $CO_2$ is then computed from Eq. (34) by multiplying for the factor $c_f$, expressed in grams of $CO_2$ per kilogram of fuel.

A graphical illustration of the vehicle module, together with the input and output quantities, is shown in Fig. 10.
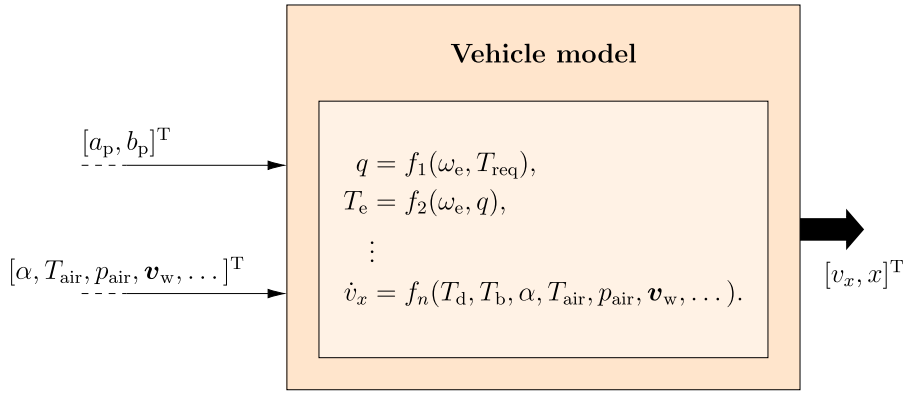
**Fig. 10.** Schematic representation of the vehicle, modelled as a system of DAEs. The inputs to the module are the acceleration and brake pedal positions $[a_p, b_p]^T$ and the $\mathscr{C}_d$ parameters in Eqs. (2). The outputs are the vehicle's longitudinal speed and position $[v_x, x]^T$. The functions $f_1(\cdot, \cdot)$ and $f_2(\cdot, \cdot)$ correspond specifically to the ones on the right-hand side of the last two Eqs. (33).

## Appendix B. Additional tables and data

Additional tables and data from the sensitivity study in Section 5 are reported here.

## References

Akin, Darcin, Sisiopiku, Virginia P., Skabardonis, Alexander, 2011. Impacts of Weather on Traffic Flow Characteristics of Urban Freeways in Istanbul. Procedia - Social and Behavioral Sciences 16, 89–99. https://doi.org/10.1016/j.sbspro.2011.04.432. URL: https://doi.org/10.10167.5C7.2Fj.sbspro.2011.04.432 (cit. on p. 4).

Amirjamshidi, Glareh, Roorda, Matthew J., 2015. Development of simulated driving cycles for light, medium, and heavy duty trucks: Case of the Toronto Waterfront Area. In: Transportation Research Part D: Transport and Environment 34, 255–266. https://doi.org/10.1016/j.trd.2014.11.010. ISSN: 1361–9209. URL: https://www.sciencedirect.com/science/article/pii/S1361920914001734 (cit. on p. 2).

Asbogaard, M., L. Johannesson, D. Angervall, and P. Johansson (2007). Improving system design of a hybrid powertrain using stochastic drive cycles and dynamic programming. In: ed. by SAE World Congress and Exhibition. Detroit, MI, USA (cit. on pp. 2, 6).

Ashatari, A., Bibeau, E., Shahidinejad, S., 2014. Using large driving record samples and a stochastic approach for real-world driving cycle construction: Winnipeg driving cycle. In: Transportation Science 48.2, 170–183. URL: https://pubsonline.informs.org/doi/abs/10.1287/trsc.1120.0447 (cit. on pp. 2, 6).

Berzi, Lorenzo, Delogu, Massimo, Pierini, Marco, 2016. Development of driving cycles for electric vehicles in the context of the city of Florence. In: Transportation Research Part D: Transport and Environment 47, 299–322. https://doi.org/10.1016/j.trd.2016.05.010. ISSN: 1361–9209. URL: https://www.sciencedirect.com/science/article/pii/S1361920916303017 (cit. on p. 3).

Bowerman, B.L., O'Connel, R., 2004. Forecasting, Time Series, and Regression, 2nd. Duxbury, North Scituate, MA (cit. on p. 9).

Box, G., Jenkins, G., Reinsel, G., Ljung, G., Ljung, G., 2015. Time Series Analysis: Forecasting and Control, 5th ed. John Wiley & Sons (cit. on pp. 8, 9).

Brady, John, O'Mahony, Margaret, 2016. Development of a driving cycle to evaluate the energy economy of electric vehicles in urban areas. In: Applied Energy 177, 165–178. https://doi.org/10.1016/j. apenergy.2016.05.094. ISSN: 0306–2619. URL: https://www.sciencedirect.com/science/article/pii/S0306261916306924 (cit. on p. 2).

C.C.C. Service (2019). Record-breaking temperatures for June, https://ucsusa.org/climate/science (cit. on p. 1).

Cadenas, Erasmo, Rivera, Wilfrido, Campos-Amezcual, Rafael, Heard, Cristopher, 2016. Wind Speed Prediction Using a Univariate ARIMA Model and a Multivariate NARX Model. In: Energies 9.2. ISSN: 1996–1073. DOI: 10.3390/en9020109. URL: https://www. mdpi.com/1996-1073/9/2/109 (cit. on p. 10).

Callery, S. (2019). Climate change: How do we know. Tech. rep. Two independence square, Washington D.C., U.S.: United States (cit. on p. 1).

Chin, Edwin H., 1977. Modeling daily precipitation occurrence process with Markov Chain. Water Resour. Res. 13 (6), 949–956. https://doi.org/10.1029/WR013i006p00949 eprint: https://agupubs. onlinelibrary. wiley.com/doi/pdf/10.1029/WR013i006p00949. URL: https://agupubs.onlinelibrary.wiley.com/doi/abs/10.1029/WR013i006p00949 (cit. on p. 9).

Donkers, Alex, Yang, Dujuan, Viktorovic, Milos, 2020. Influence ol driving style, infrastructure, weather and traffic on electric vehicle performance. In: Transportation Research Part D: Transport and Environment 88, 102569. https://doi.org/10.1016/j.trd.2020.102569. ISSN: 1361–9209. URL: https://www.sciencedirect.com/science/article/pii/S1361920920307562 (cit. on p. 3).

Erdem, Ergin, Shi, Jing, 2011. ARMA based approaches for forecasting the tuple of wind speed and direction. In: Applied Energy 88.4 1405–1414. https://doi.org/10.1016/j.apenergy.2010.10.031. ISSN: 0306–2619. URL: https://www.sciencedirect.com/science/article/pii/S0306261910004332 (cit. on p. 10).

European Commission (2014a). Regulation (eu) no 253/2014 of the european parliament and of the council of 26 february 2014 amending regulation (ec) no 510/2011 to define modalities for reaching the 2020 target to reduce co2 emissions from new light commercial vehicles, https://eur-lex. europa. eu/legal-content/EN/TXT/?uri=0J7.3AL7.3A20147.3A0847.3AT0C (cit. on p. 1).

European Commission (2014b). Regulation (eu) no 333/2014 of european parliament and of the council of 11 March 2014 amending regulation (ec) no 443/2009 to define modalities for reaching the 2020 target to reduce co2 emissions from, new passenger cars, https://eur-lex.europa.eu/legal-content/EN/TXT/?uri=0J7.3AL7.3A20147.3A0847.3AT0C (cit. on p. 1).

European Commission (2017). Commission regulation (eu) no 2017/2400. official journal of european union 60.1 247 (dec.2017). https://eur-lex. europa. eu/legal-content/EN/TXT/?uri=0J7.3AL7, 3A20177.3A3497.3AT0C (cit. on p. 1).

European Commission (2019). Vehicle Energy Consumption calculation Tool - VECTO. https://ec.europa.eu/clima/policies/transport/vehicles/vecto_en (cit. on p. 2).

European Environmental Agency (2019). Greenhouse gas emissions from transport. Tech. rep. European Environmental Agency (cit. on p. 1).

Eurostat (2019). Greenhouse gas emission statistics - emission inventories, https://ec. europa. eu/eurostat/statistics-explained/index.php/Greenhouse.gas_emission. statistics (cit. on p. 1).

Eymen, A., Koylii, U., 2019. Seasonal trend analysis and ARIMA modeling of relative humidity and wind speed time series around Yamula Dam. Meteorol Atmos Phys 131, 601–612. https://doi.org/10.1007/s00703-018-0591-8 (cit. on p. 8).

Fisher, N.I., 1993. Statistical Analysis of Circular Data. Cambridge University Press. https://doi.org/10.1017/CB09780511564345 (cit. on p. 10).

Fontaras, G., Rexeis, M., Dilara, P., Hausberger, S., Anagnostopoulos, K., 2013. he development ol a simulation tool for monitoring heavy-duty vehicle co2 emissions and luel consumption in europe. In: In: ed. by 11th International Conference on Engines and Vehicles (cit. on p.2).

G.C. Project (2017). The global carbon atlas, co2 emissions, <http://www.globalcarbonatlas.org/en/C02-emissions (cit. on p. 1).

Gabriel, K.R., Neumann, J., 1962. A Markov chain model for daily rainfall occurrence at Tel Aviv. Quarterly Journal of the Royal Meteorological Society 88 (375), 90–95. https://doi.org/10.1002/qj.49708837511 eprint: https://rmets.onlinelibrary.wiley.com/doi/pdf/10.1002/qj.49708837511. URL: https://rmets. onlinelibrary. wiley.com/doi/abs/10.1002/qj.49708837511 (cit. on p. 9).

Ghandriz, T. (2018). Transportation Mission Based Optimization of Heavy Vehicle Fleets including Propulsion Tailoring (cit. on p. 2).

Ghandriz, T., J. Hellgren, M. Islam, L. Laine, and B. Jacobson (2016). Optimization based design of heterogeneous truck fleet and electric propulsion. In: ed. by IEEE 19th International Conference on Intelligent Transportation Systems (ITSC). Rio de Janeiro, pp. 328–335 (cit. on p. 2).

Ghandriz, T., Jacobson, B., Laine, L., Hellgren, J., 2020. Impact of automated driving systems on road freight transport and electrified propulsion ol heavy vehicles. Transportation Research Part C: Emerging Technologies 115. https://doi.org/10.1016/j.trc.2020.102610 (cit. on p.2).

Guiggiani, M. (2018). The Science of Vehicle Dynamics. 2nd. Cham(Switzerland): Springer International (cit. on pp. 4, 5).

Guo, F. and F. Zhang (2016). A study of driving cycle for electric cars on Beijing urban and suburban roads. In: 2016 IEEE International Conference on Power and Renewable Energy (ICPRE), pp. 319–322. DOI: 10.1109/ICPRE.2016.7871224 (cit. on p. 8).

Guzzella, L., Sciarretta, A., 2013. Vehicle propulsion systems: introduction to modeling and optimization, 2. Springer, Berlin, Germany, 3rd.(cit. on pp. 2, 4).

Hausfather, Z. (2020). State of the climate: 2020 set to be the first ot second warmest year on record. https://www. carbonbrief.org/state-of -the- climate -2020- set -to -be -first -or- second-warmest-year-on-record (cit. on p. 1).

Heywood, J.B., 1988. Internal combustion engine fundamentals, Internat. ed. McGraw-Hill, New York, U.S (cit. on p.4).

Ho, Sze-Hwee, Wong, Yiik-Diew, Chang, Victor Wei-Chung, 2014. Developing Singapore Driving Cycle for passenger cars to estimate fuel consumption and vehicular emissions. In: Atmospheric Environment 97, 353–362. DO. https://doi.org/10.1016/j. atmosenv.2014.08.042. ISSN: 1352–2310. URL: https://www. sciencedirect.com/science/article/pii/S135223101400644X (cit. on p. 2).

Hocaoglu, Fatih Onur, Gerek, Omer Nezih, Kurban, Mehmet, 2010. A novel wind speed modeling approach using atmospheric pressure observations and hidden Markov models. In: Journal of Wind Engineering and Industrial Aerodynamics 98.8 472–481. https://doi.org/10.1016/j. jweia.2010.02.003. ISSN: 0167–6105. URL: https://www.sciencedirect.com/science/article/pii/S0167610510000255 (cit. on p. 10).

Hooper, E., Chapman, L., Quinn, A., 2013. The impact of precipitation on speed-flow relationships along a UK motorway corridor. In: Theor Appl Climatol 117, 303–316. https://doi.org/10.1007/s00704-013-0999-5. URL: https://doi.org/10.1007/s00704-013-0999-5 (cit. on p. 4).

Hsu, H.P. (2020). Schaum's Outline of Probability, Random Variables, and Random Processes. 4th. McGraw-Hill Education: New York, Chicago, San Francisco, Athens, London, Madrid, Mexico City, Milan, New Delhi, Singapore, Sydney, Toronto (cit. on p. 9).

Hung, W.T., Tong, H.Y., Lee, C.P., Ha, K., Pao, L.Y., 2007. Development of a practical driving cycle construction methodology: A case study in Hong Kong. In: Transportation Research Part D: Transport and Environment 12.2 115–128. https://doi.org/10.1016/j.trd.2007.01.002. ISSN: 1361–9209. URL: https://www. sciencedirect.com/science/article/pii/S1361920907000041 (cit. on p. 2).

Husak, Gregory J., Michaelsen, Joel, Funk, Chris, 2007. Use of the gamma distribution to represent monthly rainfall in Africa for drought monitoring applications. Int. J. Climatol. 27 (7), 935–944. https://doi.org/10.1002/joe. 1441 eprint: https://rmets. onlinelibrary. wiley.com/doi/pdf/10.1002/joe. 1441. URL: https://rmets. onlinelibrary.wiley.com/doi/abs/10.1002/joc.1441 (cit. on p. 10).

Jacobson, B., S. Berglund, and P. Pettersson (n.d.). Vehprop - a simulation model library, http://www.Chalmers.se/en/departments/m2/research/veas/Pages/ VehProp.aspx (cit. on p. 16).

Jing, Zhecheng, Wang, Guolin, Zhang, Shupei, Qiu, Chengqun, 2017. Building Tianjin driving cycle based on linear discriminant analysis. In: Transportation Research Part D: Transport and Environment 53, 78–87. https://doi.org/10.1016/j.trd.2017.04.005. ISSN: 1361–9209. URL: https://www.sciencedirect.com/science/ article/pii/S1361920916305934 (cit. on p. 3).

Johannesson, P., Podgorski, K., Rychlik, I., 2017. Laplace distribution models for road topography and roughness. In: International Journal of Vehicle Performance (IJVP) 3.3. URL: http://www. inderscience.com/off er.php?id=85032 (cit. on p. 3).

Johannesson, P., Podgorski, K., Rychlik, I., Shariati, N., 2016. AR(1) time series with autoregressive gamma variance for road topography modeling. In: Probabilistic Engineering Mechanics 34, 106–116. URL: doi-10.1016/j.probengmech.2015.12.006 (cit. on p. 3).

Kamble, Sanghpriya H., Mathew, Tom V., Sharma, G.K., 2009. Development of real-world driving cycle: Case study of Pune, India. In: Transportation Research Part D: Transport and Environment 14.2 132–140. https://doi.org/10.1016/j. trd.2008.11.008. ISSN: 1361–9209. URL: https://www.sciencedirect.com/science/article/ pii/S136192090800148X (cit. on p. 2).

Kessels, J., 2019. Traffic flow modelling. Springer. https://doi.org/10.1007/978-3-319-78695-7 (cit. on p. 11).

Kivekas, K., Vepsalainen, J., Tammi, K., 2018. Stochastic Driving Cycle Synthesis for Analyzing the Energy Consumption of a Battery Electric Bus. IEEE Access 6, 55586–55598. https://doi.org/10.1109/ACCESS.2018.2871574 (cit. on pp. 2, 3, 22).

Kivekas, K., Vepsalainen, J., Tammi, K., Anttila, J., 2017. Influence of Driving Cycle Uncertainty on Electric City Bus Energy Consumption. In: 20 17 I EEE Vehicle Power and Propulsion Conference (VPPC) 1–5.. https://doi.org/10.1109/VPPC.2017.833101 (cit. on pp. 2, 3, 22).

Kumar, V., Shanu, Jahangeer, 2017. Statistical distribution of rainfall in Uttarakhand, India. In: Appl Water Set 7, 4765–4776. https://doi.org/10.1007/sl3201-017-0586-5. URL: doi: 10.1007/sl3201-017-0586-5 (cit. on p. 10).

La Rocca, Paola, Daniele Riggi, and Francesco Riggi (Apr. 2010). Time series analysis of barometric pressure data. In: European Journal of Physics 31.3, pp. 645–655. DOI: 10.1088/0143-0807/31/3/022. URL: doi: 10.1088/0143-0807/31/3/022 (cit. on p. 9).

Lee, T., B. Adornato, and Z.S. Filipi (2011). Synthesis of Real-World Driving Cycles and Their Use for Estimating PHEV Energy Consumption and Charging Opportunities: Case Study for Midwest/U.S. In: IEEE Transactions on Vehicular Technology 60.9, pp. 4153–4163. DOI: 10.1109/TVT.2011.2168251 (cit. on p. 2).

Lee, T.K., Filipi, Z.S., 2011. Synthesis of real-world driving cycles using stochastic process and statistical methodology. In: International Journal of Vehicle Design 57.1 17–36. URL: http://www.inderscience.com/offer.php?id=43590 (cit. on p. 2, 6).

Lin, Jie, Niemeier, Debbie A, 2002. An exploratory analysis comparing a stochastic driving cycle to California's regulatory cycle. In: Atmospheric Environment 36.38 5759–5770. https://doi.org/10.1016/S1352-2310(02)00695-7. ISSN: 1352–2310. URL: https://www.sciencedirect.com/science/article/pii/ S1352231002006957 (cit. on pp. 2, 3).

Liu, L., C. Huang, M. Liu, and S. Shi (2008). Study on the Combined Design Method of Transient Driving Cycles for Passenger Car in Changchun. In: 2009 IEEE Vehicle Power and Propulsion Conference. URL: https://ieeexplore. ieee.org/stamp/stamp. jsp?arnumber=4677594 (cit. on p. 2).

Liu, X., J. Ma, X. Zhao, J. Du, and Y. Xiong (2020). Study on Driving Cycle Synthesis Method for City Buses considering Random Passenger Load. In: Journal of Advanced Transportation. DOI: 10.1155/2020/3871703. URL: doi: 10.1155/2020/3871703 (cit. on pp. 2, 3).

Liu, Y., M.C. Roberts, and R. Sioshansi (2018). A vector autoregression weather model for electricity supply and demand modeling. In: Journal of Modern Power Systems and Clean Energy 6.4, pp. 763–776. DOI: 10.1007/s40565-017-0365-l (cit. on p. 8).

Llopis-Castello, David, Ana Maria Perez-Zuriaga, Francisco Javier Camacho-Torregrosa, and Alfredo Garcia (2018). Impact of horizontal geometric design of two-lane rural roads on vehicle co2 emissions. In: Transportation Research Part D: Transport and Environment 59, pp. 46–57. ISSN: 1361–9209. doi: 10.1016/j.trd.2017. 12.020. URL: https://www.sciencedirect.com/science/article/pii/S1361920917303164 (cit. on p. 2).

Mastinu, G., Ploechl, M., 2014. Road and of-road vehicle system dynamics handbook, 1st. CRC Press, FL, U.S (cit. on p.4).

Naghizadeh, M. (2003). DEVELOPMENT OF CAR DRIVE CYCLE FOR SIMULATION OF EMISSIONS AND FUEL ECONOMY. In: (cit. on p.2).

Nesamani, K.S. and K.P. Subramanian (2011). Development of a driving cycle for intra-city buses in Chennai, India. In: Atmospheric Environment 45.31, pp. 5469–5476. ISSN: 1352–2310. doi: 10.1016/j.atmosenv.2011.06.067. URL: https://www.sciencedirect.com/science/article/pii/S1352231011006911 (cit. on p. 2).

Nyberg, P. (2015). Evaluation, generation and transformation of driving cycles. PhD thesis. Linkoping, Sweden (cit. on p. 2).

Ou, S., Y. Zhou, L. Lian, P. Jia, and B. Tian (2011). Development of hybrid city bus's driving cycle. In: 2011 International Conference on Electric Information and Control Engineering, pp. 2112–2116. DOI: 10.1109/ICEICE.2011.5777149 (cit. on p. 3).

Pacejka, H.B. (2012). Tyre and vehicle dynamics. 3rd. Oxford, UK: Elsevier/Butterworth-Heinemann (cit. on pp. 4, 5).

Perugu, Harikishan (2019). Emission modelling of light-duty vehicles in India using the revamped VSP-based MOVES model: The case study of Hyderabad. In: Transportation Research Part D: Transport and Environment 68. Urbanization, Transportation and Air Quality in Developing Countries, pp. 150–163. ISSN: 1361–9209. doi: 10.1016/j. trd.2018.01.031. URL:https://www.sciencedirect.com/science/article/pii/S1361920917301104 (cit. on p. 2).

Pettersson, P., 2019. Operating cycle representation for road vehicles. PhD thesis. Chalmers University of Technology (cit. on pp. 3-6).

Pettersson, P., S. Berglund, B.J. Jacobson, L. Fast, P. Johannesson, and F. Santandrea (2019). A proposal for an operating cycle description format for road transport missions. In: European Transport Research Review 10.31, pp. 1–19. URL: doi: 10.1186/sl2544-018-0298-4 (cit. on pp. 3, 30).

Pettersson, P., Jacobson, B., Berglund, S., 2016. A model of an automatically shifted truck for prediction of longitudinal performance on an operating cycle. Tech. rep. Chalmers University of Technology (cit. on p. 16).

Pettersson, P., B. Jacobson, F. Bruzelius, P. Johannesson, and L. Fast (2020). Intrinsic differences between backward and forward vehicle simulation models. In: IFAC-PapersOnLine 53.2.21th IFAC World Congress, pp. 14292–14299. ISSN: 2405–8963. doi: 10.1016/j. if acol.2020.12. 1368. URL: https://www.sciencedirect.com/science/article/pii/S2405896320317754 (cit. on p. 3).

Pettersson, P., P. Johannesson, B. Jacobson, F. Bruzelius, L. Fast, and S. Berglund (2019). A statistical operating cycle description for prediction of road vehicles' energy consumption. In: Transportation Research Part D: Transport and Environment 73, pp. 205–229. URL: doi: 10.1016/j.trd.2019.07.006 (cit. on pp. 3-7, 12, 13, 16).

Rakha, Hesham, Kyoungho Ahn, and Antonio Trani (2004). Development of VT-Micro model for estimating hot stabilized light duty vehicle and truck emissions. In: Transportation Research Part D: Transport and Environment 9.1, pp. 49–74. ISSN: 1361–9209. doi: 10.1016/S1361 - 9209 (03) 00054 - 3. URL: https://www.sciencedirect.com/science/article/pii/S1361920903000543 (cit. on p. 1).

Romano, Luigi, Bruzelius, Fredrik, Jacobson, Bengt, 2020. Brush tyre models for large camber angles and steering speeds. Vehicle System Dynamics 1–52. https://doi.org/10.1080/00423114.2020.1854320. URL: https://doi.org/10.1080/00423114.2020.1854320 (cit. on p. 5).

Romano, Luigi, Bruzelius, Fredrik, Jacobson, Bengt, 2020. Unsteady-state brush theory. Vehicle System Dynamics 1–29. https://doi.org/10.1080/00423114.2020. 1774625. URL: https://doi.org/10.1080/00423114.2020. 1774625 (cit. on p. 5).

Romano, Luigi, Bruzelius, Fredrik, Jacobson, Bengt, 2021. A Brush Tyre Model with Standstill Handler for Energy Efficiency Studies. In: In: Commercial Vehicle Technology 2020/2021. Proceedings. https://doi.org/10.1007/978-3-658-29717-6_10 (cit. on p. 16).

Sciarretta, A. (2020). Energy-Efficient Driving of Road Vehicles. Springer (Cham), Springer Nature Switzerland AG. URL: doi: 10.1007/978-3-030-24127-8 (cit. on pp. 2, 11).

Sentoff, K., L. Aultman-Hall, and B. Holme (2015). Implications of driving style on road grade for accurate vehicle data and emissions estimates. In: Transportation Research Part D: Transport and Environment 35, pp. 175–188. URL: doi: 10.1016/j.trd.2014.11.021 (cit. on p. 2).

Shi, S., N. Lin, Y. Zhang, C. Huang, L. Liu, B. Lu, and J. Cheng (2013). Research on Markov Property Analysis of Driving Cycle. In: 2013 IEEE Vehicle Power and Propulsion Conference (VPPC), pp. 1–5. DOI: 10.1109/VPPC.2013.6671737 (cit. on p. 3).

Shi, S., S. Wei, H. Kui, L. Liu, C. Huang, and M. Liu (2009). Improvements of the design method of transient driving cycle for passenger car. In: 2009 IEEE Vehicle Power and Propulsion Conference, pp. 1581–1586. DOI: 10.1109/VPPC.2009.5289594 (cit. on p. 2).

Silvas, E., 2015. Integrated optimal design for hybrid electric vehicles. English. Proefschrift. PhD thesis. In: Department of Mechanical Engineering, 2. ISBN: 978-90-386-3968-0 (cit. on pp. 2, 3). Nov.

Silvas, E., Hereijgers, K., Peng, H., Hofman, T., Steinbuch, M., 2016. Synthesis of Realistic Driving Cycles With High Accuracy and Computational Speed, Including Slope Information. IEEE Trans. Veh. Technol. 65 (6), 4118–4128. https://doi.org/10.1109/TVT.2016.2546338 (cit. on pp. 2, 3).

Song, Guohua, Lei, Yu., Yizheng, Wu., 2016. Development of Speed Correction Factors Based on Speed- Specific Distributions of Vehicle Specific Power for Urban Restricted-Access Roadways. Journal of Transportation Engineering 142 (3), 04016001. DOI: 10.1061/(ASCE)TE. 1943-5436.0000819. eprint: https://ascelibrary.org/doi/pdf/10.1061/%28ASCE%29TE. 1943-5436.0000819. URL: https://ascelibrary.org/doi/abs/10.1061/7.5C7.28ASCE7.5C7.29TE. 1943-5436.0000819 (cit. on pp. 20, 22).

Tazelaar, Edwin, Bruinsma, Jogchum, Veenhuizen, Bram, Van den Bosch, Paul, 2009. Driving cycle characterization and generation, for design and control of fuel cell buses. World Electric Vehicle Journal 3 (4), 812–819. https://doi.org/10.3390/wevj3040812. URL: https://www.mdpi.com/2032-6653/3/4/812 (cit. on p. 2).

Tennekes, H., 1973. The Logarithmic Wind Profile. Journal of Atmospheric Sciences 30 (2), 234–238. https://doi.org/10.1175/1520-0469(1973)030<0234:TLWP.0. C0;2. URL: https://journals.ametsoc.org/view/journals/atsc/30/2/1520-0469_1973_030_0234_tlwp_2_0_co_2.xml (cit. on p. 13).

U.S.E.P. Agency (2019). Overview of greenhouse gases. Tech. rep. Two independence square, Washington D.C., U.S.: United States: Environmental Protection Agency (cit. on p. 1).

Union of concerned scientists (2019). Global warming. Tech. rep. Cambridge, MA, U.S (cit. on p. 1).

Vepsalainen, Jari, Klaus Kivekas, Kevin Otto, Antti Lajunen, and Kari Tammi (2018). Development and validation of energy demand uncertainty model for electric city buses. In: Transportation Research Part D: Transport and Environment 63, pp. 347–361. ISSN: 1361–9209. doi: 10.1016/j. trd.2018.06.004. URL: https://www.sciencedirect.com/science/article/pii/S1361920917308301 (cit. on p. 3).

Wong, J., 2008. Theory of ground vehicles.4th. John Wiley & Sons, Hoboken, NJ, U.S (cit. on p. 4).

Wyatt, D.W., H. Li., and J.E. Tate (2014). The impact of road grade on carbon dioxide (co2) emissions of passenger vehicle in real-world driving. In: Transportation Research Part D: Transport and Environment 32, pp. 160–170. URL: doi: 10.1016/j.trd.2014.07.015 (cit. on p. 2).

Zou, Zhanjiang, Davis, Scott, Beaty, Kevin, O`Keele, Michael, Hendricks, Terry, Rehn, Robert, Weissner, Steve, Sharma, V.K., 2004. A New Composite Drive Cycle for Heavy-Duty Hybrid Electric Class 4–6 Vehicles. In: In: SAE Technical Paper. SAE International. https://doi.org/10.4271/2004-01-1052. Mar. (cit. on p. 2).